doi:10.1093/brain/awt341 Brain 2014: 137; 707–723 | 707

BRAIN
A JOURNAL OF NEUROLOGY

Toll-like receptor 2-mediated alternative activation of microglia is protective after spinal cord injury

David P. Stirling,[1,2] Karen Cummins,[1] Manoj Mishra,[1] Wulin Teo,[1] V. Wee Yong[1] and Peter Stys[1]

1 Department of Clinical Neurosciences, Hotchkiss Brain Institute, University of Calgary, Calgary, Alberta Canada
2 Kentucky Spinal Cord Injury Research Centre and Departments of Neurological Surgery, Microbiology and Immunology, University of Louisville, Louisville, KY, USA

Correspondence to: David P. Stirling, Ph.D.
Assistant Professor
Departments of Neurological Surgery,
Microbiology and Immunology
KY Spinal Cord Injury Research Centre
University of Louisville
511 S. Floyd Street, MDR Bld., Rm. 608
Louisville, KY 40292, USA
E-mail: david.stirling@louisville.edu

Improving neurological outcome after spinal cord injury is a major clinical challenge because axons, once severed, do not regenerate but 'dieback' from the lesion site. Although microglia, the immunocompetent cells of the brain and spinal cord respond rapidly to spinal cord injury, their role in subsequent injury or repair remains unclear. To assess the role of microglia in spinal cord white matter injury we used time-lapse two-photon and spectral confocal imaging of green fluorescent protein-labelled microglia, yellow fluorescent protein-labelled axons, and Nile Red-labelled myelin of living murine spinal cord and revealed dynamic changes in white matter elements after laser-induced spinal cord injury in real time. Importantly, our model of acute axonal injury closely mimics the axonopathy described in well-characterized clinically relevant models of spinal cord injury including contusive-, compressive- and transection-based models. Time-lapse recordings revealed that microglia were associated with some acute pathophysiological changes in axons and myelin acutely after laser-induced spinal cord injury. These pathophysiological changes included myelin and axonal spheroid formation, spectral shifts in Nile Red emission spectra in axonal endbulbs detected with spectral microscopy, and 'bystander' degeneration of axons that survived the initial injury, but then succumbed to secondary degeneration. Surprisingly, modulation of microglial-mediated release of neurotoxic molecules failed to protect axons and myelin. In contrast, sterile stimulation of microglia with the specific toll-like receptor 2 agonist Pam2CSK4 robustly increased the microglial response to ablation, reduced secondary degeneration of central myelinated fibres, and induced an alternative (mixed M1:M2) microglial activation profile. Conversely, *Tlr2* knock out: *Thy1* yellow fluorescent protein double transgenic mice experienced greater axonal dieback than littermate controls. Thus, promoting an alternative microglial response through Pam2CSK4 treatment is neuroprotective acutely following laser-induced spinal cord injury. Therefore, anti-inflammatory treatments that target microglial activation may be counterintuitive after spinal cord injury.

Keywords: microglia; spinal cord injury; axonal dieback; TLR2; myelin

Abbreviations: KO = knock out; SCI = spinal cord injury; TLR = toll-like receptor; YFP = yellow fluorescent protein

Received July 12, 2013. Revised October 21, 2013. Accepted October 25, 2013. Advance Access publication December 24, 2013

Introduction

Microglia respond rapidly to injury; however, their role in acute secondary white matter injury or repair after spinal cord injury (SCI) remains poorly understood. Live imaging studies have shown that microglia survey their environment and respond within minutes to injury (Davalos *et al*., 2005; Nimmerjahn *et al*., 2005); this response may be beneficial because inhibiting microglial process extension results in larger lesions in brain slices (Hines *et al*., 2009). Furthermore, transplanting microglia (Prewitt *et al*., 1997; Rabchevsky and Streit, 1997) or macrophages (Rapalino *et al*., 1998) after CNS insult or stimulating macrophages with Toll-like receptor (TLR) agonists (e.g. zymosan) improves axonal sprouting/regeneration in some paradigms (Leon *et al*., 2000; Ahmed *et al*., 2010; Hauk *et al*., 2010).

In contrast, numerous studies have shown that microglia and blood-derived macrophages release potent neurotoxins after injury (e.g. reactive oxygen species; nitric oxide and the formation of peroxynitrite; cytokines such as TNF-alpha and IL1B; and glutamate) (Giulian *et al*., 1993; Satake *et al*., 2000; Taylor *et al*., 2003; Bao *et al*., 2004; Yawata *et al*., 2008). In support, activation of microglia/macrophages through TLRs induces neuronal cell death and neurite degeneration (Fitch *et al*., 1999; Lehnardt *et al*., 2002; Popovich *et al*., 2002). As white matter elements are sensitive to these neurotoxins, treatments aimed at reducing the microglial/macrophage response and subsequent neurotoxicity are often protective (Blight, 1994; Popovich *et al*., 1999; Park *et al*., 2004; Domercq *et al*., 2007; Byrnes *et al*., 2009) and prevent the second late phase of axonal dieback (Stirling *et al*., 2004; Horn *et al*., 2008).

TLRs, a large family of pattern recognition receptors, respond to both 'danger' and 'stranger' signals (Kawai and Akira, 2010). TLR2 and TLR4 signalling in microglia/macrophages induces these cells to secrete pro-inflammatory cytokines as well as other potentially toxic molecules (Lehnardt, 2010). Based on these divergent roles of microglia/macrophages in CNS injury, we hypothesized that specifically targeting microglia in isolation of monocyte-derived macrophages, by inhibiting their neurotoxic release of glutamate and other inflammatory factors, would protect spinal cord white matter. Conversely, stimulating microglia by potent TLR agonists would promote white matter injury.

Two-photon excitation time-lapse video microscopy revealed that the microglial response spatially and temporally correlated with ongoing secondary degeneration (i.e. axonal dieback and secondary 'bystander' degeneration of axons that survived the initial ablation but later succumbed to axonal degeneration). Remarkably, treatments that have previously been shown to reduce microglial-mediated glutamate release and reduce their neurotoxicity, failed to protect axons or prevent their dieback following laser-induced SCI. Conversely stimulating microglia with the specific TLR2 agonist Pam2CSK4, but not other TLR receptor agonists, augmented the microglial response to laser-induced SCI, polarized microglia to an alternative protective (mixed M1:M2) phenotype, and preserved white matter elements.

Taken together, these observations suggest that microglial responses in isolation after SCI are ineffective at protecting vital white matter elements. However, their typical activation states can be boosted and biased towards a beneficial profile through specific TLR2 agonists. A better understanding of the mechanisms behind these divergent TLR2 stimulated responses and which stimuli result in beneficial reactions, will potentially guide therapeutic interventions to improve neurological outcome after SCI.

Materials and methods

Ex vivo whole spinal cord model

All experiments were conducted in accordance with the University of Calgary Animal Care Ethics Committee, adhering to the guidelines of the Canadian Council on Animal Care. Adult 6–8 week old heterozygous *Cx3cr1*$^{GFP/+}$ mice (Jung *et al*., 2000) (a kind gift from Dr Paul Kubes) were used to visualize microglia, *Thy1*YFP^{+} mice (Feng *et al*., 2000) (a kind gift from Dr Douglas Zochodne) were used to visualize dorsal column axons, or *Cx3cr1*$^{GFP/+}$: *Thy1*YFP^{+} double transgenic mice bred in house to visualize both microglia and axons simultaneously, were used for all imaging experiments. The transgenic mice were backcrossed to C57BL/6 mice for at least 10 generations. *Tlr2*-knockout (*Tlr2*KO) mice (a kind gift from Dr Paul Kubes) were bred in-house with *Thy1*YFP^{+} to produce *Tlr2*KO:*Thy1*YFP+ double transgenic mice and *Tlr2*wildtype:*Thy1*YFP+ double transgenic mice littermate controls used for all experiments. Genotyping confirmed the genotype of all mice in the experiments. Mice were deeply anaesthetized with an intraperitoneal injection of sodium pentobarbital (Ceva Sante Animale) and perfused transcardially (1 ml/min) with ice cold low Ca^{2+} artificial CSF (in mM: NaCl 126, $NaHCO_3$ 26, KCL 3, NaH_2PO_4 1.25, $MgSO_4$ 2, $CaCl_2$ 0.1, and dextrose 10) bubbled in 95% O_2/5% CO_2 to remove blood and keep the spinal cord viable during the dissection. After the removal of the skin and hair, an incision was made through the skull and a multi-segment laminectomy was made using forceps and fine scissors to expose the dorsal surface of the spinal cord from the brainstem to the lumbar region without damaging the underlying myelinated fibres. Using a fine-tipped scalpel blade, the spinal cord at the mid-thoracic level and at the level of the brainstem was transected. After transection, the underlying vertebral column was cut to isolate the spinal cord and supported by a vertical slice to clamp the exposed bones within a customized imaging chamber (RC-27L Large Bath Chamber, Harvard Apparatus) (Supplementary Fig. 1). The spinal cord was then continuously perfused (~1.5 ml/min) for the remainder of the imaging experiments in normal 2 mM Ca^{2+} artificial CSF bubbled with 95% O_2/5% CO^2, and maintained at 36.5°C through an in-line heater equipped with temperature feedback control (Harvard Apparatus) and an objective heater system (Bioptechs Inc.) (Supplementary Fig. 1). Using this set-up, the *ex vivo* spinal cord remained viable for up to 12 h after injury. To visualize myelin, the lipophilic dye Nile Red (N-1142, Life Technologies Inc.) was dissolved in dimethyl sulphoxide and used at a final concentration of 25 μM, then directly and briefly added to the perfusion chamber. To eliminate oversaturation or to avoid poor myelin labeling, Nile Red was added directly to the perfusion chamber in 2-μl volumes, left for 2–5 min to penetrate the spinal cord, and repeated until adequate and specific labelling of myelin was achieved. Once the initial labelling of myelin was achieved, Nile Red was added once again at 2 h after laser-induced SCI until clear labelling of myelin surrounding yellow fluorescent protein (YFP)-positve axon profiles was achieved. Importantly, using this experimental perfusion system, the spinal cord in isolation

remained viable up to 12 h after laser-induced SCI based on morphological observation of axons, myelin and microglia (data not shown).

Microscopy

Time-lapse two-photon excitation images of fluorescently labelled samples were obtained by using a custom-modified commercial system (Nikon D-Eclipse C1, Nikon Instruments). Spinal cords were then excited with 50-fs pulses with wavelengths of 950 nm (GFP, YFP and Nile Red) at 10–15 mW generated by a Ti:sapphire laser (Tsunami, Spectra-Physics Lasers) through a water-immersion objective ×60 1.0 NA, Fluor (Nikon) for visualizing fluorescent proteins and dyes. The fluorescence emitted was filtered through 525/25 nm band-pass and 590 nm long-pass filters (Chroma Technologies) to a pair of photomultiplier tubes for detection (Hamamatsu R5929).

For some preparations, after two-photon excitation imaging, the chamber containing the spinal cords were transferred to a Nikon C1si spectral laser scanning confocal microscope to collect spectral data (emission spectra separated into 32 bins) of fluorescent proteins and dyes using the ablation site as a reference. As Nile Red, our lipophilic vital myelin probe, undergoes solvatochromism dependent on its chemical environment, we took advantage of this property to assess changes in myelin and axons after injury. We noted that transected axonal endbulbs, but not normal axons fluoresce brightly with Nile Red and the emission maxima was shifted to 630 nm compared with myelin and adipocytes (emission maxima 580–90 nm). These Nikon files were also imported into Imagetrak software and 'unmixed' using the spectral manager function of the software (written by P.K.S.). Thus, using our unmixing algorithm overlapping emission spectra such as GFP and YFP could be easily separated as long as the emission maxima were separated by 10 nm. Similarly, Nile Red shifts >10 nm could be unmixed in a similar fashion.

Laser-induced spinal cord injury

Baseline time-lapse recordings of the middle of the cervical enlargement were obtained 30 min to 1 h after initial alignment under the two-photon microscope. Using Nikon software (EZ-C1), the area of the proposed ablation site was magnified ×11.9 (17.81 × 17.81 μm, area = 317.20 μm^2) and the laser wavelength tuned to 800 nm, 50–75 mW for 10 passes (1.92 μs pixel dwell time), to produce a highly focal and intense laser pulse to completely transect dorsal column axons. After ablation, the laser wavelength was tuned to 950 nm and power reduced to 10–15 mW as detailed above for time-lapse recordings.

Pharmacological agents

Lipopolysaccharide (TLR4 agonist, 100 ng/ml) and zymosan A (TLR2/dectin-1 agonist, 100 ng/ml) were purchased from Sigma; Pam2CSK4 (TLR2 agonist, 100 ng/ml) was purchased from InvivoGen; carbenoxolone (a gap junction blocker, 200 μM, used to prevent glutamate release; Yawata *et al*., 2008), L-AP4, a selective group III metabotropic glutamate receptor agonist, 100 μM, to prevent microglial release of neurotoxins (Taylor *et al*., 2003), cycloheximide (selective inhibitor of protein synthesis, 50 μM) were purchased from Tocris. These agents were then solubilized, diluted and stored as per manufacturer's recommendations. All pharmacological agents were added at the indicated concentrations and continuously perfused 30 min before laser-induced SCI until 4 h after laser-induced SCI. The concentration of agonists was approximated based on what was previously used to elicit responses in myeloid cells *in vitro* (Pinteaux-Jones *et al*., 2008; Yawata *et al*., 2008; Long *et al*., 2009). For example both lipopolysaccharide and Pam2CSK4 at 100 ng/ml (as used in the present study) induced activation of MAP kinase and NF-κB signalling pathways and inflammatory cytokine expression in the murine macrophage/monocyte cell line Raw 264.7, and bone marrow-derived macrophages from C57BL/6 mice (Long *et al*., 2009). Importantly, the effects of Pam2CSK4 were TLR2 specific as Pam2CSK4 was unable to induce activation of the above signalling pathways in macrophages from *Tlr2*$^{-/-}$ mice (Long *et al*., 2009). However, assessment of a more extensive dose range of the agonists used in the study should be the focus of future experiments to compliment these studies.

Image analysis

To quantify axonal dieback, ablation width, ablation area, and width of axon loss ('bystander' loss of adjacent axons), time-lapse recordings of the entire ablation field were collected in z-stacks (0.6 μm/step size; 0.174 μm/pixel) at baseline, 2 min, 5 min, 30 min, 1 h, 2 h, 3 h and 4 h after laser-induced SCI and the 4D image data were then imported into ImageTrak (written by P.K.S.) for visualization and analysis on a Macintosh OS X computer. Image stacks were autoregistered to reduce movement artefacts caused during image acquisition. The distance of dieback of individual axons proximal (caudal) to the ablation site over time was measured using a distance tool. Only endbulbs that were clearly connected to a proximal axonal stalk were included in the analysis to avoid including fragments of degenerating axons. The distance between the endbulb and the ablation edge was recorded. A total of n = 39–141 axonal endbulbs per group, from 4–14 animals per group, were analysed and expressed as median and 25th and 75th percentile (box and whisker plots). As Nile Red reliably labelled the ablation site and the ablation site did not change over 4 h after laser-induced SCI, we measured the ablation width and area using a distance and area tool respectively, on five individual adjacent images centred over the middle of the ablation over time. A total of n = 14–26 ablation sites from 14–26 animals were analysed and expressed as mean ± SEM. To quantify 'bystander' loss of axons adjacent to the ablation site that survived the initial injury, but then succumbed to secondary degeneration, we measured the width of axonal loss using a distance tool on individual images at the centre of the ablation site. The width of axonal loss was calculated as the total lesion width (distance between the closest intact axons on both sides of the ablation site) minus the ablation site width (contains primary injured axons). A total of n = 4–14 ablation sites from 4–14 animals per group were analysed and expressed as mean ± SEM. All experimenters that analysed images in this study were blind to treatment. See Table 1 for a complete description of each group used for image analysis. As each vehicle control for each treatment group had slightly different solvents and no differences were determined between the different solvents they were pooled for analysis.

Microglia quantification

To quantify the microglial response to laser-induced SCI, we used a similar approach to document the microglial response in the brain (Davalos *et al*., 2005). Similar to the microglial response to brain injury, spinal cord white matter microglia respond to laser-induced SCI by rapidly orientating their processes towards the ablation site to surround or seal of the injury. Time-lapse recordings from each treatment group were opened in ImageTrak software and maximum intensity plots were created from baseline, 2 min, 5 min, 30 min, 1 h, 2 h, 3 h, and 4 h following laser-induced SCI. The maximum intensity plots were produced from the centre of the laser ablation site as determined

Table 1 Number of subjects and *n* used for image analysis in the study

Analysis	Subjects	*n*	Treatment
Ablation area	26	26	All treatment groups
Width of axonal loss	14	14	All artificial CSF controls
Ablation width	14	14	All artificial CSF controls
Microglial response	5	5	Artificial CSF
Microglial response	4	4	Pam2CSK4
Microglial response	4	4	Lipopolysaccharide
Microglial response	4	4	L-AP4
Microglial response	4	4	Zymosan
Endbulb distance	14	141	All artificial CSF controls
Endbulb distance	4	87	Pam2CSK4
Endbulb distance	4	90	Lipopolysaccharide
Endbulb distance	4	105	L-AP4
Endbulb distance	4	39	Zymosan
Endbulb distance	4	77	*Tlr2*KO
Bystander axonal loss	14	14	All artificial CSF controls
Bystander axonal loss	4	4	Pam2CSK4
Bystander axonal loss	4	4	Lipopolysaccharide
Bystander axonal loss	4	4	L-AP4
Bystander axonal loss	4	4	Zymosan
Bystander axonal loss	4	4	*Tlr2*KO
Bystander axonal loss	4	4	Carbenoxolone
Bystander axonal loss	4	4	Cycloheximide

in the *z*-plane and included a total of 17 sections surrounding the ablation site with a *z*-step size of 0.6 μm giving a total depth of 10.2 μm. To subtract Nile Red signal leakage within the green (GFP) channel, image math was performed on all images using the following formula, green channel = g − (25 × r), where g = GFP channel and r = Nile Red channel. This approach greatly reduced Nile Red leakage signal within the green channel to allow for a purer collection of true microglial signal. A mask channel (blue) was then used to threshold all the images uniformly to maximize signal to noise in the green channel. The maximum intensity plots from each time-point was then analysed as follows. Using a circular poly tool in ImageTrak, three circles were created on the maximum intensity plots to outline the ablation site (ablation poly, 40-μm diameter to subtract fluorescence signal from the ablation), adjacent to the lesion site (*x*-poly, 75-μm diameter) to assess the movement of microglia processes towards the edges of the lesion and an outer ring poly (*y*-poly, 100-μm diameter) to determine the starting microglial position. We then calculated the microglial response to laser-induced SCI using the following formula: Microglia response = R(t) = (Rx(t) − Rx(0) / Ry(0), where x = inner shell y = outer shell t = time, 0 = baseline. Four to five spinal cords per treatment group were compared.

Quantitative polymerase chain reaction

At 4 h after laser-induced SCI, the dorsal columns containing the ablation site from *n* = 3–4 animals/group were flash frozen in liquid N_2 and stored at −80°C before use. The tissue samples for RNA were homogenized in TRIzol® reagent (Invitrogen) using, successively, 20 G and 25 G needles and stored at −80°C prior to use. RNA was extracted using the RNeasy® Mini Kit columns (Qiagen), and for quantitative PCR, RNA was first treated with DNase (Promega) and reverse transcribed using SuperScript® II reverse transcriptase (Invitrogen). The resulting complementary DNA was used as a template for the BioRad iCycler detection system and 2× SYBR green mastermix (Qiagen). Every primer (10× QuantiTect Primer Assay) that was used was purchased from Qiagen and details can be found on their website. Expression of gene transcripts were normalized against the housekeeping gene, *GAPDH*. Relative expression levels for our genes of interest were determined using the formula $2^{-\Delta CT}$ where ΔCT = CT (gene of interest) − CT (housekeeping gene).

Flow cytometry

At 4 h after laser-induced SCI, cells from the dorsal columns that contained the ablation site were separated into neural and leucocyte populations by discontinuous density gradient centrifugation using isotonic Percoll® (GE Healthcare). CNS cell samples were prepared at 4°C in buffer solution (fluorescence-activated cell sorting buffer) and stained with antibodies against CD45, CD11b and Ly6C. The percentage of pro-inflammatory microglia (M1, CD45low, $CDllb^+$, $Ly6C^{high}$) were compared between sham and treatments groups (*n* = 3–4/group). Antibodies and their isotype controls were purchased from BD Bioscience. Isotype controls were always included in the assays. Cells were incubated for 45 min in a combination of directly conjugated antibodies at 4°C. Data acquisition was performed on a flow cytometer (BD FACSAria; BD Biosciences) and analysed with FlowJo (TreeStar) software blind to treatment group.

Statistics

All treatment groups were compared and graphs produced using SigmaPlot 11 (Systat Software, Inc.). Axonal dieback data were tested using a Kruskal-Wallis one-way ANOVA on Ranks with Dunn's method of multiple comparisons versus artificial CSF control group as the data failed normality. Width of axonal loss was compared between groups using an ANOVA, with a Holm Sidak multiple comparisons versus artificial CSF control or in the case of normality or equal variance test failure, Kruskal-Wallis one-way ANOVA on Ranks with Dunn's method of multiple comparisons versus artificial CSF control group was used. Ablation area, ablation width, and width of axonal loss from artificial CSF-treated spinal cords were compared over time using a repeated measures ANOVA and multiple comparisons versus control group (Holm-Sidak method). For the microglial response, quantitative PCR, and flow cytometry, treatment groups were compared using an ANOVA and multiple comparisons versus control group (Holm-Sidak method). $P < 0.05$ was considered statistically significant.

Results

Microglia and central myelinated fibre response to laser-induced spinal cord injury

We developed an *ex vivo* laser-induced SCI model to isolate the microglial response from blood-derived immune cells to directly assess the microglial response to injury without confounding

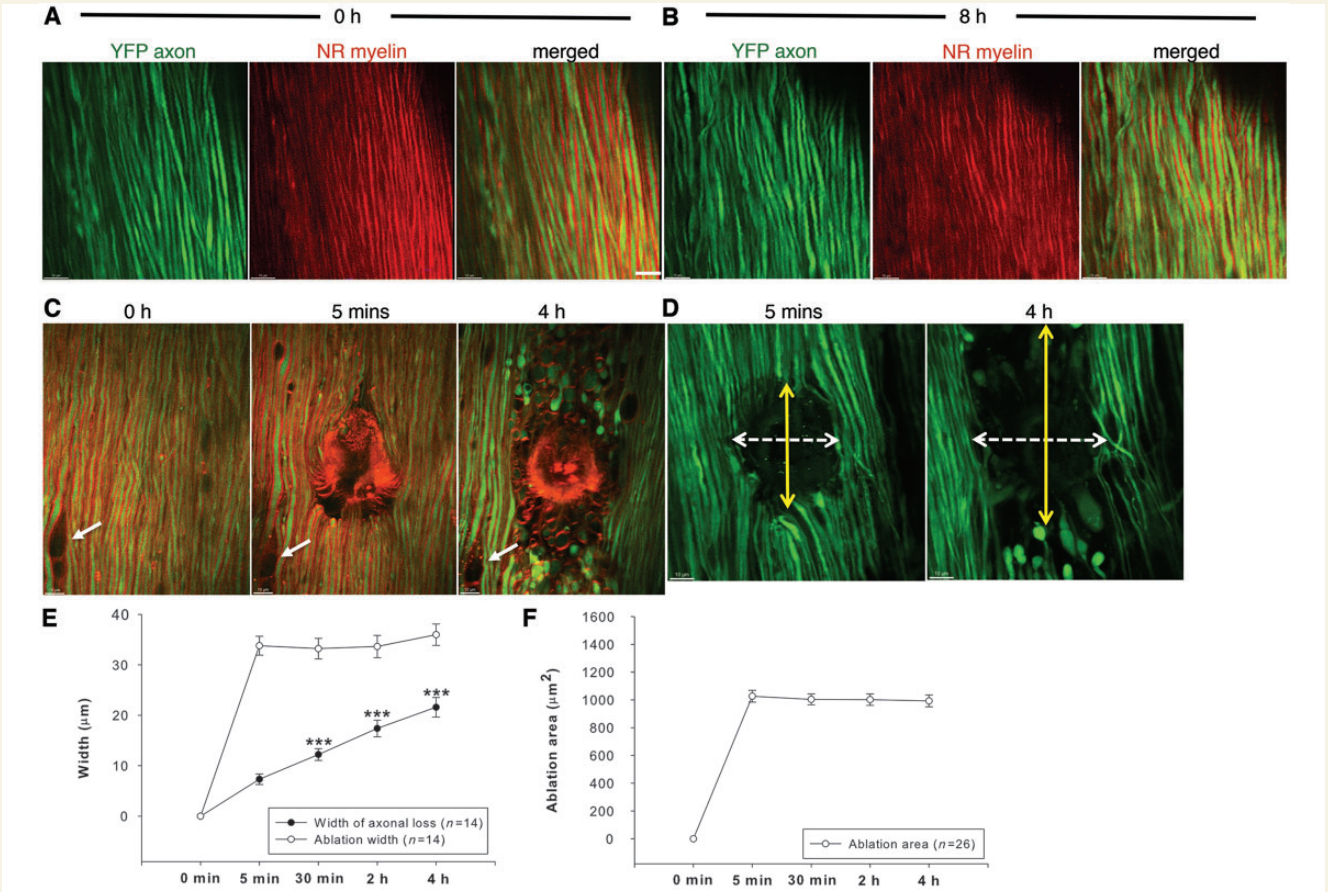

Figure 1 Laser-induced SCI causes axonal dieback and secondary axonal degeneration. Two-photon excitation time-lapse recordings of the dorsal surface of the living spinal cord from 0 h (**A**) to 8 h (**B**) revealed parallel-aligned dorsal column axons [green, YFP positive ensheathed in myelin; red, Nile Red (NR)] with few morphological signs of degeneration. (**C**) Laser-induced SCI induced axonal dieback and fibre loss adjacent to the ablation site that increased over time (merged images of YFP and Nile Red). White arrows indicate a glial cell and is used as a spatial reference point. (**D**) Representative images clearly demonstrate axonal dieback from 5 min to 4 h (yellow arrows) after laser-induced SCI, whereas white arrows represent an increase in axonal loss adjacent to the ablation site. Notably, the width of the ablation site of primary immediate injury [**E**, ablation width (open circles) and area (open circles, **F**)] does not significantly ($P > 0.05$) change over time allowing the distinction between primary and secondary injury in real time. In distinction, secondary 'bystander' axonal loss (width of axonal loss minus the ablation width) significantly increases over time (filled circles, **E**). Data are represented as mean ± SEM, One-way repeated measures ANOVA,***$P < 0.001$, $n = 14$ animals in **E** and $n = 26$ animals in **F**. Scale bar = 10 μm.

effects from blood-derived macrophages. By combining two-photon excitation and spectral confocal microscopy to spectrally 'unmix' closely spaced fluorescent probes, we documented changes in axons, microglia and myelin after injury in real-time using heterozygous transgenic mice that express GFP in microglia (*Cx3cr1*$^{GFP/+}$), YFP in axons (*Thy1*YFP+) or double transgenic mice (*Cx3cr1*$^{GFP/+}$:*Thy1*YFP+). Normal myelin, damaged myelin, and transected axonal endbulbs were visualized by application of the solvatochromic fluorescent dye Nile Red, which undergoes emission spectra changes dependent on its environment, and used here for the first time to detect underlying axo-glial injury.

Live imaging of dorsal column fibres from cervical spinal cord revealed YFP$^+$ axon profiles ensheathed in myelin (Nile Red) that appeared morphologically normal in naïve control conditions up to 8 h after ablation (Fig. 1A and B). To reliably transect a discrete number of dorsal column fibres we performed laser-induced SCI. An area measuring ~20 × 20 μm on the dorsal surface of the spinal cord was irradiated 10 times in rapid succession with 800 nm pulsed light at 600 mW (measured at the scanhead) creating a well-defined and reproducible lesion. The transected axons (primary injury) formed swollen endbulbs both rostral and caudal to injury and retracted up to 100 μm during a standard 4-h observation period (Fig. 1C). In addition, fibres adjacent to the ablation site that survived the initial injury later succumbed to secondary 'bystander' degeneration (Fig. 1D). Importantly, the width of secondary axonal loss significantly ($P < 0.001$) increased from 5 min (7.33 ± 1.05 μm, mean ± SEM) to 4 h (21.60 ± 1.95 μm) after laser-induced SCI representing an ~195% increase in spared adjacent fibre loss at 4 h (Fig. 1E). These data suggest that substantial numbers of axons that

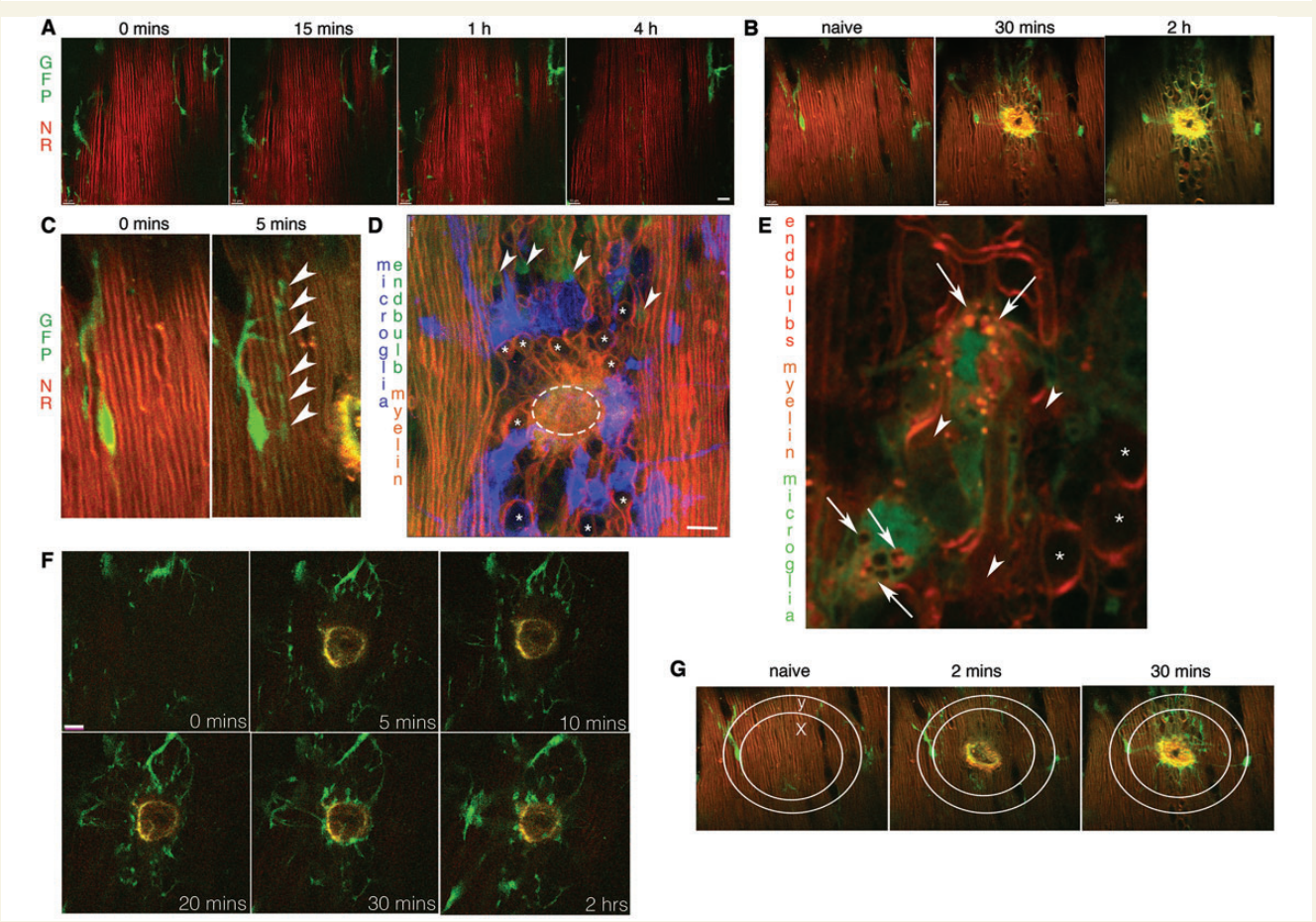

Figure 2 Laser-induced SCI induces a microglial response in close association with delayed axonal degeneration. (**A**) Representative two-photon excitation images from time-lapse recordings of living spinal cord reveal highly ramified microglia (GFP+, green) and normal appearing myelin [red, Nile Red (NR)] in control conditions over time. (**B** and **C**) In contrast, microglia (green) rapidly respond to laser-induced SCI and orient their processes (arrowheads) towards the lesion site (yellow). (**D**) Spectral 'unmixing' of overlapping spectra from fluorescent proteins and lipophilic dyes (see 'Materials and methods' section) at the ablation site (dashed circle) after laser-induced SCI. Microglia (blue, GFP) are in close proximity to myelin spheroids (asterisk Nile Red, orange) and intimately contact actively retracting endbulbs (Nile Red emission maximum to 630 nm, shown in green, arrowheads). Myelin (orange, Nile Red emission maximum 580 nm) further lateral to the ablation, but not adjacent to the lesion appears normal and is mostly unassociated with microglia. (**E**) High magnification image showing microglia (green) in close proximity to retracting axonal endbulbs (red, Nile Red, arrowheads) and myelin spheroids (asterisk). The use of Nile Red shows that microglia engage in myelin phagocytosis forming internal phagolysosomes (arrows) after laser-induced SCI. (**F**) Images from time-lapse recordings of microglia (green) and their response to laser-induced SCI (yellow) over time. (**G**) We quantified the microglial response to injury by measuring the density of microglial signal that accumulates in an inner circle 'x' from an outer circle 'y' as the microglia extend their processes to seal off the ablation site over time (see 'Materials and methods' section). Scale bars = 10 μm.

survived the original laser ablation succumbed to secondary degeneration in a delayed fashion. Importantly, we were able to follow this dynamic response using time-lapse microscopy and clearly distinguish between primary versus secondary injured axons as the primary injury site, did not change ($P = 0.25$, $P = 0.55$, respectively) over time (Fig. 1E and F).

Under control conditions, microglia (GFP^+) were highly ramified and frequently extended/retracted their processes parallel to ascending myelinated fibres (Fig. 2A) (Davalos *et al.*, 2005; Nimmerjahn *et al.*, 2005; Dibaj *et al.*, 2010). In contrast, microglia in the vicinity of laser-induced SCI responded within minutes by orienting and directing their processes towards the ablation site (Fig. 2B, C and F; Supplementary Video 1). Using spectral confocal imaging and subsequent 'unmixing' of multiple overlapping fluorescent proteins and dyes using algorithms generated by P.K.S (see 'Materials and methods' section and Fig. 3), we were able to document that microglial processes (GFP^+) were in intimate contact with retracting axonal end bulbs (red-shifted protein staining of Nile Red; Figs 2D and 3), damaged ballooning myelin (Nile Red), and clearly phagocytosed myelin debris (Fig. 2E). Microglia were also localized to degenerating YFP-positive axons (spectral unmixing of YFP axons and GFP microglia; Fig. 3A-D) and contacted myelin spheroids and retracting axonal endbulbs (Fig. 3E–H). Thus, recordings of live spinal white matter revealed

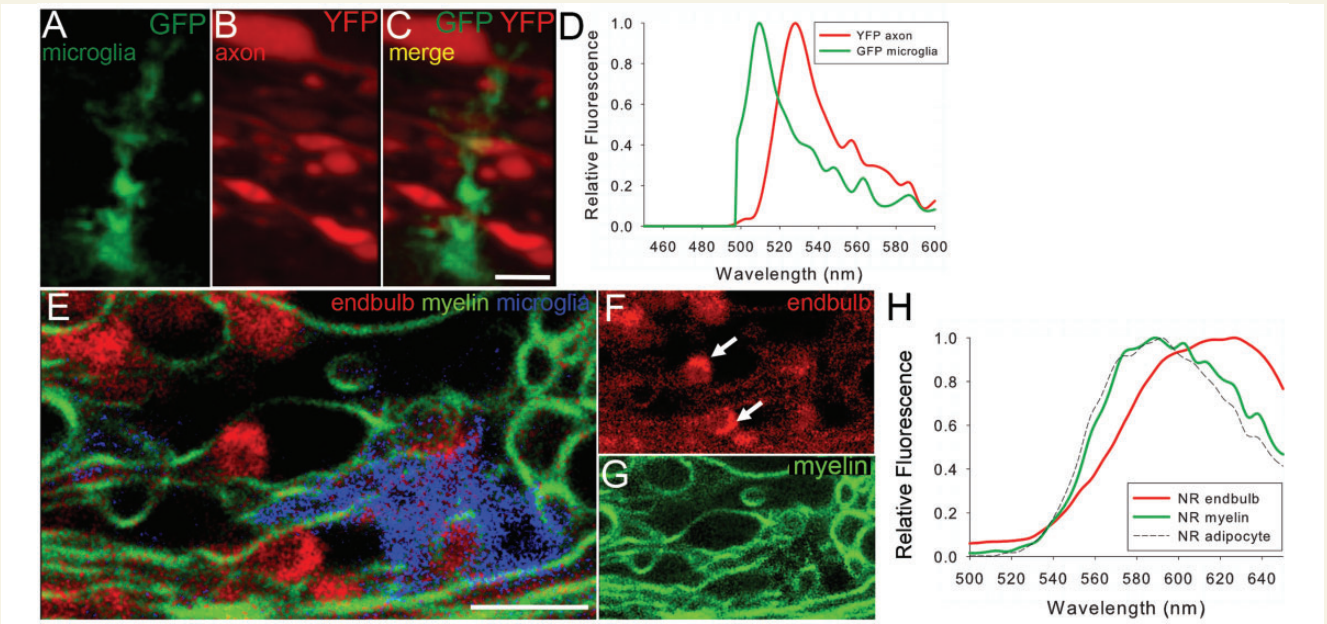

Figure 3 Spectral 'unmixing' of overlapping spectra of fluorescent proteins and dyes. (**A–C**) Spectral images of the living dorsal surface of the spinal cord from *Cx3cr1*GFP/+: Thy1YFP+ double transgenic mice at 4 h after a laser-induced SCI, captured with an Eclipse C1si spectral confocal microscope (Nikon). A microglial cell (GFP+, green) in the presence of degenerating axons (YFP+, red), merge of **A** and **B** in **C**. Scale bar = 10 μm. The emission spectra from the two fluorescent proteins are shown in **D**: note the extensive degree of spectral overlap that would be difficult to separate using conventional dichroics and emissions filters. Each pixel in the resulting spectral image contained 32 channels of spectrally resolved data that was loaded into our unmixing algorithm (written by P.K.S.). (**E–G**) Spectral images of the living dorsal surface of the spinal cord from a *Cx3cr1*GFP/+ transgenic mouse stained with the lipophilic solvatochromic Nile Red (NR) and captured at 4 h after laser-induced SCI. Nile Red undergoes spectral shifts dependent on the chemical environment in which the dye is exposed to and these shifts can be 'unmixed' even if their emission maxima are separated by only 10 nm. Nile Red's emission spectrum is blue-shifted in the less polar, more lipid-rich environment of adipocytes (hashed line, **H**) and normal CNS myelin (green, **E–H**). In contrast, Nile Red's emission spectrum peaks at ~625 nm [~40–50 nm shift compared to normal myelin (~580–590 nm)] in axonal endbulbs undergoing axonal dieback suggestive of underlying changes in protein accumulation or disorganization revealing presumably hydrophobic binding sites (red, **E–H**). Microglia (blue) are shown in close proximity to myelin spheroids (Nile Red, green) and axonal endbulbs (Nile Red shifted, red) and may influence secondary myelin and axonal degeneration after injury. Representative images and emission spectra from $n = 5$ mice. Scale bar = 10 μm.

that reactive microglia (shorter, thicker processes) were intimately associated with myelin (Nile Red) and axons (spectral shift Nile Red) undergoing pathophysiological changes within the first 4 h after laser-induced SCI, a pattern that was not observed during baseline conditions.

Effects of microglial modulation on the microglial response to laser-induced spinal cord injury

To prevent microglial-mediated white matter injury we targeted microglial release of neurotoxic molecules using the group III metabotropic glutamate receptor agonist L-AP4, and glutamate release through gap junctions with carbenoxolone. Conversely, stimulating microglia with potent sterile pro-inflammatory TLR agonists (e.g. lipopolysaccharide, TLR4 agonist; zymosan, TLR2/dectin-1 receptor agonist) that have been previously shown to increase glutamate, nitric oxide, free radical, and cytokine release from microglia/macrophages would augment white matter injury (Fitch *et al.*, 1999; Lehnardt *et al.*, 2002; Popovich *et al.*, 2002; Takeuchi *et al.*, 2005). As zymosan can activate both TLR2 and dectin-1 receptors (Brown *et al.*, 2003) we also assessed the pure synthetic lipopeptide, Pam2CSK4, as a specific and potent activator of TLR2 receptors (van Bergenhenegouwen *et al.*, 2013). The treatment groups are detailed in Table 1.

As shown in Fig. 4, the mean microglial response to laser-induced SCI was robustly enhanced by pretreatment (30 min) with TLR agonists. Specifically, the Pam2CSK4-stimulated microglial response doubled from 2 min (13.30 ± 2.86; mean response ± SEM) and remained significantly increased up to 4 h (27.00 ± 5.23) after laser-induced SCI when compared with artificial CSF controls (3.42 ± 0.78 and 9.93 ± 1.51 at 2 min and 4 h, respectively, $n = 4$ per treatment group, $P < 0.05$) (Fig. 4A and B and Supplementary Video 2). Lipopolysaccharide modulation also significantly increased the microglial response to laser-induced SCI versus artificial CSF controls from 2 h until 4 h after laser-induced SCI (lipopolysaccharide, 31.51 ± 2.35; artificial CSF, 9.93 ± 1.51, $n = 4$ per group, $P < 0.05$), albeit in a delayed manner compared with Pam2CSK4 treatment (Fig. 4A and B). In contrast to these

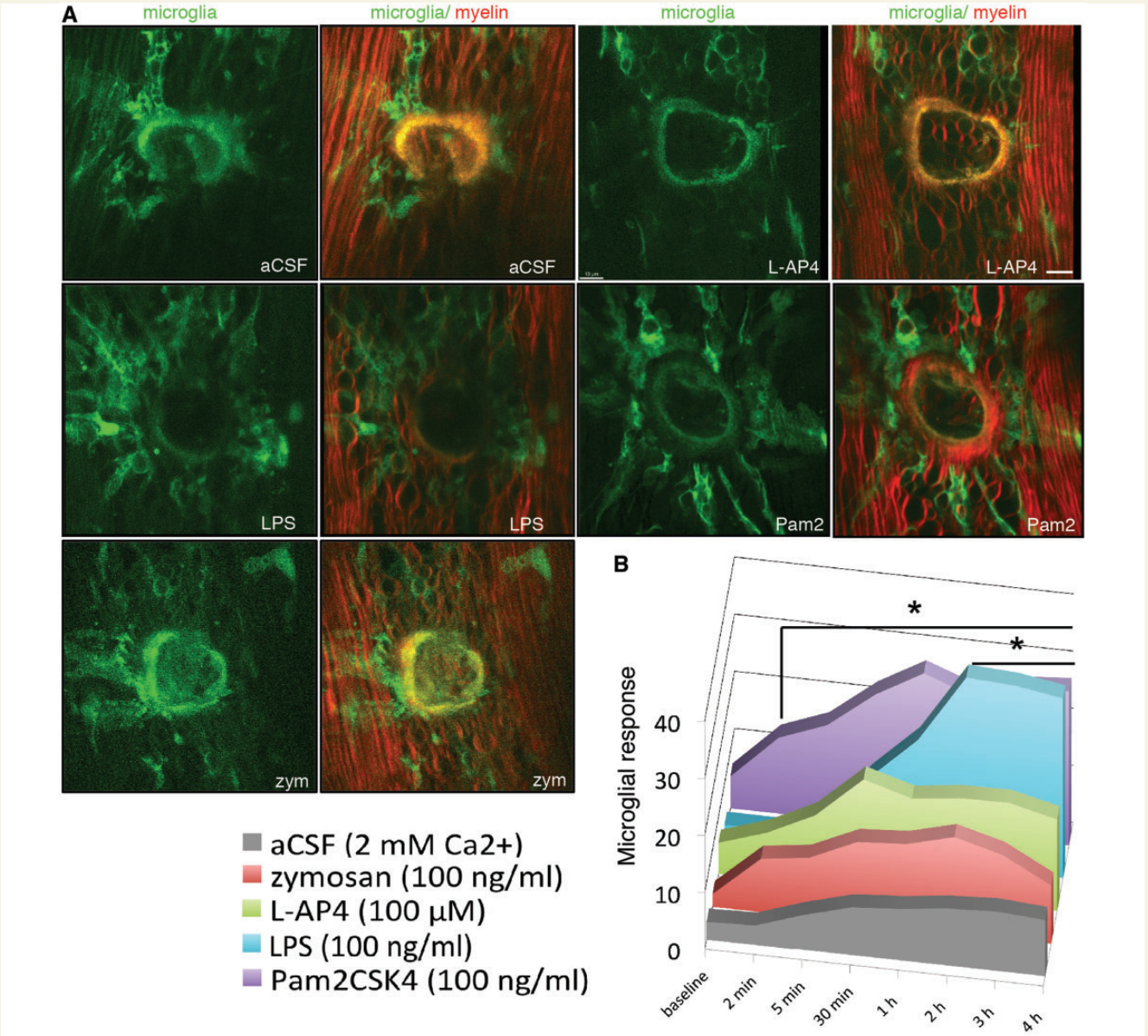

Figure 4 Pam2CSK4 and lipopolysaccharide modulation of microglia increases the microglial response to laser-induced SCI. (**A**) Representative images from two-photon excitation time-lapse recordings at 4 h after laser-induced SCI in control, artificial CSF (aCSF), L-AP4, lipopolysaccharide (LPS), Pam2CSK4 (Pam2), and zymosan (zym)-treated spinal cords collected at the ablation site (yellow). The microglial response (GFP, green), and myelin (red, Nile Red) are shown. Merged images of microglia/myelin are shown to the right of the image. Scale bar = 10 µm. (**B**) Quantification of the microglial response to laser-induced SCI. Before laser-induced SCI there were no significant differences ($P = 0.19$) in the microglial response between any of the microglial modulators compared to artificial CSF controls. The specific TLR2 agonist Pam2CSK4 significantly ($P < 0.01$) increased the microglial response to laser-induced SCI at 2 min through to 4 h after laser-induced SCI versus controls. Lipopolysaccharide stimulation increased ($P < 0.05$) the microglial response to injury in a delayed manner compared with Pam2CSK4 treatment, beginning at 2 h until 4 h after injury. Neither zymosan or L-AP4 altered the microglial response ($P > 0.05$). Data are represented as mean ± SEM, $n = 4–5$ animals per group. One-way ANOVA, Holm-Sidak method of multiple comparisons versus control group. *$P < 0.05$.

results, L-AP4, carbenoxolone (data not shown), zymosan, or cycloheximide (data not shown) pretreatment did not significantly alter the microglial response to laser-induced SCI versus artificial CSF controls. These data support the concept that the microglial response (timing and quantity of microglial process extension) to laser-induced SCI can be enhanced effectively using specific TLR2 and -4 agonists.

Effects of microglial modulation on acute axonal dieback following laser-induced spinal cord injury

Unlike peripheral axons, most transected central spinal axons form non-regenerative 'endbulbs' at their distal tip and die back away

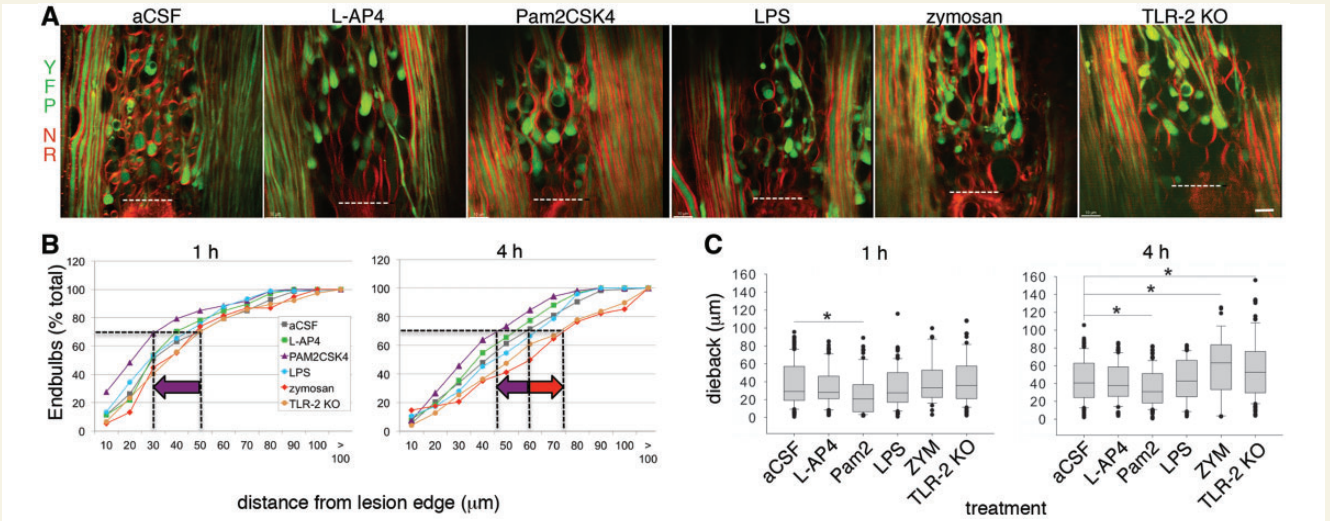

Figure 5 Pam2CSK4 modulation of microglia reduces proximal axonal dieback after laser-induced SCI. (**A**) Representative two-photon excitation images of YFP + axons (green) and myelin [Nile Red (NR), red] from timelapse recordings of the dorsal surface of the cervical spinal cord *ex vivo* at 4 h after laser-induced SCI. Laser-induced SCI induces proximal axonal dieback of transected (primary injury) axons away from the lesion edge (dashed line). Scale bar = 10 μm. (**B**) Cumulative distribution plots of axonal dieback at 1 h and 4 h after laser-induced SCI. Treatments that reduce axonal dieback shift the distribution curve to the left (indicated by the purple arrow for Pam2CSK4). Treatments that increase axonal dieback shift the curve to the right (red arrow, zymosan; *Tlr2*KO:YFP + double transgenic mice) compared with artificial CSF (aCSF) controls. (**C**) Box and whisker plots of axonal dieback distance at 1 h and 4 h after laser-induced SCI. Pam2CSK4 significantly reduced axonal dieback at both 1 and 4 h after laser-induced SCI. Zymosan and *Tlr2*KO: YFP + double transgenic mice revealed significantly increased axonal dieback at 4 h after injury. Data are represented as median, 25th, 75th percentile of proximal dieback distance for each treatment group. Kruskal-Wallis one-way ANOVA on Ranks, Dunn's method of multiple comparisons versus control group, $n = 39–141$ axons per treatment group, from 4–14 animals per group. $^*P < 0.05$.

from the lesion epicentre after SCI. Although the precise mechanisms that mediate axonal dieback after SCI remain unknown, anti-inflammatory treatment of SCI-rats with minocycline or methylprednisolone reduced both the CNS macrophage response and the late phase of axonal dieback (Oudega *et al*., 1999; Stirling *et al*., 2004). Furthermore, clodronate liposome-mediated depletion of blood-derived macrophages prior to SCI confirmed a role for macrophages in mediating late phase axonal dieback (Horn *et al*., 2008). However, whether microglial cells *per se* contribute to SCI-induced acute or late phase axonal dieback remains unknown.

To examine the role of microglia in acute axonal dieback we applied microglial modulators and quantified axonal dieback over time by recording the distance between the ablation edge and the endbulbs utilizing two-photon excitation time-lapse video microscopy. Only endbulbs in continuity with their proximal axons were included in our analysis to rule out axons undergoing acute Wallerian-like degeneration. The latter were easily distinguishable from actively retracting axons as fragmented axonal segments were discontinuous in the z-plane and had faded YFP expression. Unexpectedly, microglial stimulation by the TLR2 agonist Pam2CSK4, that robustly increased the microglial response to laser-induced SCI and in distinction to the other microglial modulators, significantly reduced proximal axonal dieback (Fig. 5A–C). Representative images from two-photon excitation time-lapse recordings 4 h after laser-induced SCI are shown for each of the treatment groups and *Tlr2*KO: *Thy1*YFP$^+$ double transgenic mice (Fig. 5A). Cumulative distribution of endbulbs as a function of distance from the lesion edge at 1 h and 4 h (Fig. 5B) revealed that Pam2CSK4 treatment shifts the distribution curves to the left, i.e. less axonal retraction/dieback, whereas both *Tlr2*KO:*Thy1*YFP$^+$ double transgenic mice and zymosan treatment shifted the curve to the right suggestive of greater axonal retraction versus control (artificial CSF) (Fig. 5B). Quantitation of these results confirmed that Pam2CSK4 treatment significantly reduced proximal axonal dieback at 1 h and 4 h following laser-induced SCI compared to artificial CSF treated controls whereas zymosan and *Tlr2*KO:*Thy1*YFP$^+$ double transgenic mice significantly worsened axonal retraction (Fig. 5C). In contrast to these results, microglial modulation with L-AP4, cycloheximide (data not shown) or carbenoxolone (data not shown) did not prevent axonal dieback. Indeed, the latter induced robust acute Wallerian-like degeneration (pan-fragmentation) of the transected fibres within the first 2 to 4 h after laser-induced SCI (Fig. 6).

Together, these results suggest that inducing a robust microglial response with the specific TLR2 agonist Pam2CSK4, but not zymosan or lipopolysaccharide, greatly reduces laser-induced SCI-induced axonal dieback; a necessary prerequisite for growth cone formation and subsequent axonal regeneration. Conversely, treatments that target microglial glutamate release were ineffective at reducing axonal dieback. Furthermore, the exacerbated axonopathy in *Tlr2*KO:*Thy1*YFP$^+$ double transgenic mice at 4 h after laser-induced SCI likely contributes to the worsened neurological outcome in *Tlr2*KO mice after contusion SCI (Kigerl *et al*., 2007).

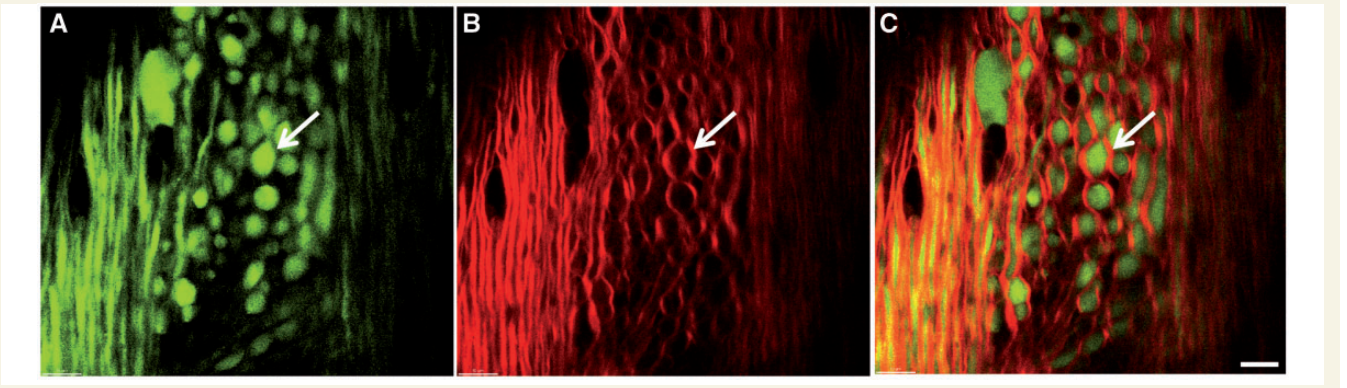

Figure 6 Inhibiting microglial release of glutamate with carbenoxolone does not protect white matter elements after laser-induced SCI. Based on previous literature that has shown that carbenoxolone treatment prevents microglia/macrophage release of glutamate (Yawata *et al*., 2008), we applied carbenoxolone to inhibit microglial release of glutamate. Surprisingly, carbenoxolone (200 μM) continuously perfused beginning 30 min before laser-induced SCI did not protect axons or myelin. Instead axons underwent massive pan-fragmentation [**A**, YFP+ (axon fragments green); one arrow is shown for clarity] tightly enclosed in myelin enclosures (**B**, Nile Red, red). (**C**) Merge of **A** and **B**. Representative images from one animal spinal cord is shown from $n = 4$ animals. Scale bar = 10 μm.

Effects of microglial modulation on secondary 'bystander' degeneration of spared axons after laser-induced spinal cord injury

To further examine the neuroprotective effects of Pam2CSK4 we measured the width of axonal loss (i.e. 'bystander' loss) of adjacent axons that survived the primary injury but succumbed to secondary degeneration over time as revealed by time-lapse recordings of the ablation site. As shown in Fig. 7, Pam2CSK4 treatment significantly reduced secondary 'bystander' degeneration of adjacent fibres at 30 min and 4 h (Pam2CSK4; 13.06 ± 1.413, mean ± SEM) after laser-induced SCI compared to artificial CSF controls (21.6 ± 1.95) (Fig. 7A and B). In contrast, zymosan, a TLR2/dectin-1 receptor antagonist increased lesion width at 5 min after laser-induced SCI and continued a strong trend to an increase in bystander loss of axons from 30 min to 4 h after injury (Fig. 7A and B). Similarly to zymosan, *Tlr2*KO:*Thy1*YFP$^+$ double transgenic mice experienced an acute increase in the width of axonal loss compared to artificial CSF controls; however, this did not reach significance. Lipopolysaccharide, a TLR4 agonist, despite greatly increasing the microglial response to laser-induced SCI (Fig. 3), did not prevent myelinated fibres from undergoing secondary degeneration (Fig. 7A and B). Neither microglia modulation with the group III metabotropic glutamate receptor receptor agonist L-AP4, that has been previously shown to promote a protective microglia phenotype; carbenoxolone, that has been previously shown to reduce microglial glutamate release; nor cycloheximide, an inhibitor of protein synthesis, prevented bystander loss of myelinated fibres acutely after laser-induced SCI (Fig. 7C).

Effects of microglial modulation on microglial phenotype

Given the beneficial effects on white matter sparing by stimulating microglia with Pam2CSK4, we next assessed whether microglial modulation altered their pro-inflammatory repertoire. Research in models of infection and disease support the concept that macrophages can be polarized to classical (M1, pro-inflammatory) or alternative (M2, anti-inflammatory) activated states (Gordon, 2003). In the SCI setting, M1 macrophages dominate the lesion site and remain elevated up to 6 weeks after SCI, whereas M2 macrophages are scarce at later time points (Kigerl *et al*., 2009). Blocking M1 recruitment promotes alternatively activated M2 macrophage recruitment and improves neurological outcome after SCI (Guerrero *et al*., 2012). However, whether true microglia heterogeneity *per se* exists or whether they can be polarized after SCI and the resultant outcome on destructive or reparative processes remains unclear. Towards this goal, we prepared single cell preparations of spinal cord white matter from sham, Pam2CSK4-treated and endotoxin-free water control-treated dorsal columns at 4 h after laser-induced SCI and assessed the amount of inflammatory microglia (CD45^{low}:CD11b$^+$:Ly6C$^+$) between the different treatment groups by flow cytometry (Stirling and Yong, 2008) (Figs 8 and 9). As shown in Figs 8 and 9A, laser-induced SCI did not increase the total amount of spinal white matter microglia (CD45^{low}:CD11b$^+$) over sham controls at the 4-h time point, neither did it divide the population into distinct Ly6C^{high} (M1) or Ly6C^{low} (M2) populations as has been shown for monocytes (Mishra *et al*., 2012). However, laser-induced SCI significantly increased the percentage of CD45^{low}:CD11b$^+$:Ly6C$^+$ pro-inflammatory microglial cells compared to sham controls at 4 h after injury. Intriguingly, Pam2CSK4 treatment significantly ($P < 0.001$) reduced the amount of CD45^{low}:CD11b$^+$:Ly6C$^+$ microglial cells versus endotoxin-free water controls (Figs 8 and 9A). In contrast, neither laser-induced SCI nor Pam2CSK4 treatment altered the CD45^{high}:CD11b$^+$ Ly6C$^+$ CNS macrophage population (Figs 8 and 9B). As no circulating cells are present in our *ex vivo* spinal cord model, these CD45^{high} cells may represent microglia with increased CD45 expression or perivascular/leptomeningeal cells included in the preparation.

We next assessed cytokine and M1, M2 marker expression profiles isolated from the spinal cord 4 h after laser-induced SCI.

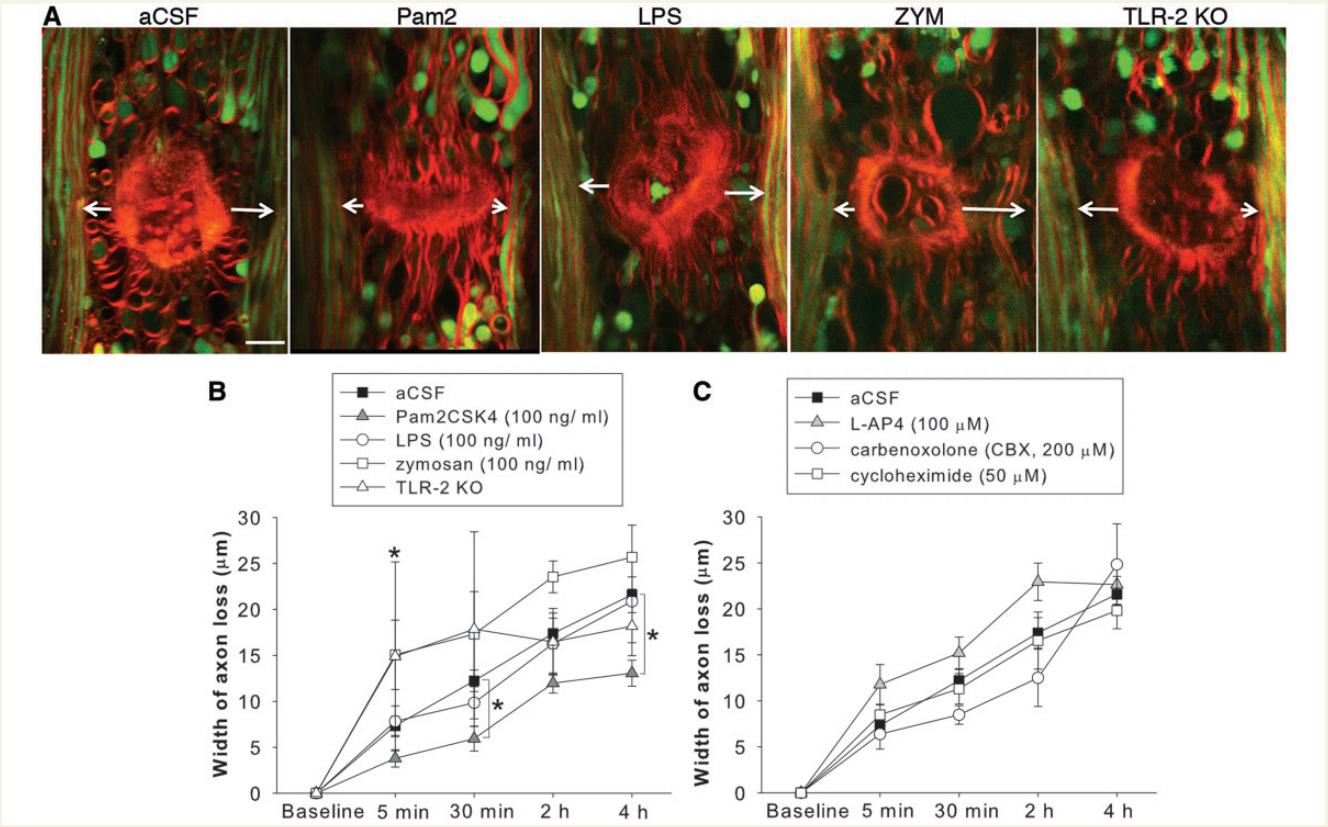

Figure 7 Pam2CSK4 modulation of microglia reduces secondary 'bystander' loss of myelinated fibres after laser-induced SCI. (**A**) Representative two-photon excitation images of YFP+ axons (green) and myelin (Nile Red, red) from time-lapse recordings at 4 h after laser-induced SCI. Laser-induced SCI induces secondary 'bystander' degeneration of myelinated fibres adjacent to ablation site (red circle in centre of image). Scale bar = 10 μm. The white arrows indicate the amount of secondary axonal loss adjacent to the lesion. (**B** and **C**) Quantitation of axonal loss (secondary 'bystander' axonal degeneration), as a function of time after laser-induced SCI. Pam2CSK4 treatment significantly reduced lesion width at 30 min and 4 h after injury compared with artificial CSF (aCSF) controls (**B**). The TLR2/dectin-1 agonist, zymosan (ZYM), significantly increased lesion width at 5 min after laser-induced SCI. Lipopolysaccharide (LPS) stimulation of TLR4 receptors did not alter lesion width compared with controls. (**C**) Inhibiting the microglial response with L-AP4, carbenoxolone or cycloheximide did not reduce bystander loss of axons after laser-induced SCI. Data are represented as mean ± SEM for each treatment group. Statistical significance was assessed using a one-way ANOVA with Holm-Sidak method for multiple comparisons or in the case of unequal variances, a Kruskal-Wallis one-way ANOVA on Ranks with Dunn's method of multiple comparisons. $n = 4–14$ spinal cords per treatment group. $^*P < 0.05$.

As shown in Fig. 9C, several markers of inflammation were altered after laser-induced SCI. Specifically, inflammatory markers CCL2, IL1-beta, inducible nitric oxide synthase, SOCS1 and 3, and IL-1ra were significantly elevated in Pam2CSK4-treated spinal cords versus sham controls and inducible nitric oxide synthase, SOCS3 and IL-1ra were significantly increased in Pam2CSK4 treated spinal cords versus laser-induced SCI controls (Fig. 9C). Interestingly, markers of the M2 alternative activation pathway (arginase 1, IL-10, mannose receptor, CD206) were 2 to 3-fold higher in Pam2CSK4-treated cords versus laser-induced SCI controls, however, only SOCS3 and IL-1ra levels reached significance. Pam2CSK4-treatment reduced the laser-induced SCI-induced increase in Ly6C expression in microglia, a marker of classically activated monoctyes (M1), and altered the inflammatory milieu following laser-induced SCI. We found very little evidence of a true M1 versus M2 phenotype in microglia but rather an 'alternative' activation profile within the two extremes where both M1 (inducible nitric oxide synthase) and M2 (SOCS3, IL-1ra) markers were elevated acutely with treatment. Pam2CSK4 applied to sham controls did not affect gene expression.

Collectively, Pam2CSK4 treatment robustly increased the microglial response to laser-induced SCI and reduced axonal dieback and secondary 'bystander' loss of axons adjacent to the lesion site. Moreover, Pam2CSK4 treatment altered the inflammatory milieu of microglia (less Ly6C+ expressing microglia), cytokine and M1, M2 marker expression by inducing concurrent pro-inflammatory and anti-inflammatory molecules that together promote white matter sparing after laser-induced SCI. Thus treatments designed to inhibit the microglial response to white matter injury seem counter-intuitive when both the inflammatory response and effects on white matter sparing are assessed in real-time acutely after injury.

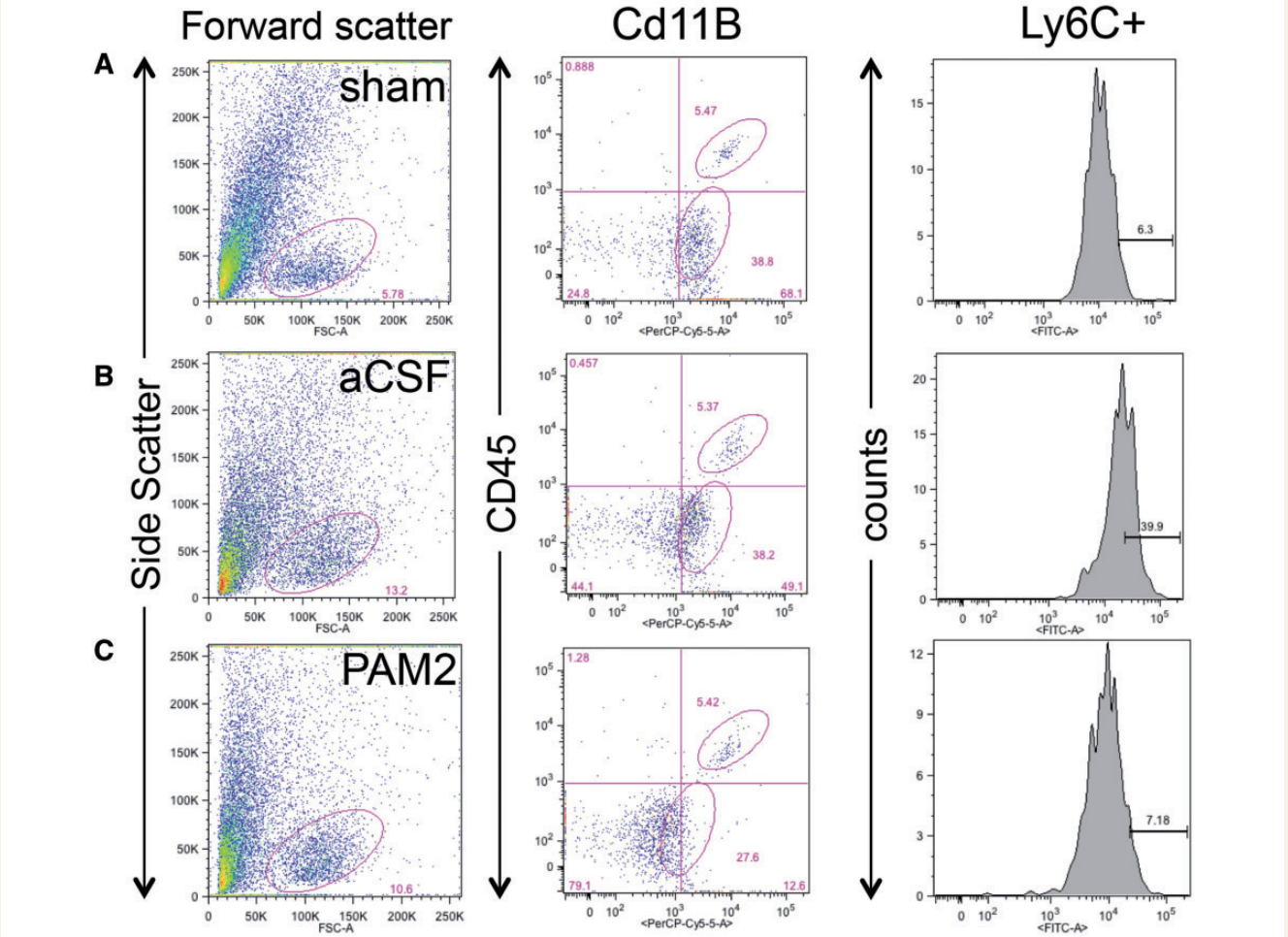

Figure 8 Pam2CSK4 Treatment reduces microglial ($CD45^{low}$:CD11b+) expression of the M1 pro-inflammatory marker Ly6C. Single cell suspensions of myeloid cells were prepared from laser-induced SCI dorsal column white matter at 4 h after injury and subjected to flow cytometric analysis. (**A**) Sham uninjured spinal cord, (**B**) laser-induced SCI controls (artificial CSF with endotoxin-free water), and (**C**) laser-induced SCI Pam2CSK4 (PAM2) treatment. Representative light scatterplots from each of the groups is shown (side scatter, *y*-axis: forward scatter, *x*-axis, far left) and the gates used to quantify CD45low:CD11b positive microglia (bottom ellipse, *middle* panel) and CD45high:CD11b positive macrophages (top ellipse, *middle* panels) as determined from isotype controls (not shown). Plots of Ly6C+ microglia from the population of CD45low:CD11b microglia are shown on the far right for each treatment group. Total counts of the population of microglia that express Ly6C high levels are shown for the various treatment groups. Representative plots and histograms from a total of $n = 4$ animals/group.

Discussion

After CNS trauma microglia are rapidly recruited to the site of injury followed by the recruitment of neutrophils and subsets of blood-derived macrophages that populate the lesion site over time (Dusart and Schwab, 1994; Kigerl *et al*., 2009). In addition, perivascular macrophages and leptomeningeal macrophages likely add to this global myeloid response to injury once the protective CNS barriers are breached. The function of these divergent myeloid populations, their temporal and spatial (lesion border versus lesion cavity) accumulation, arsenal of potential neurotoxic and wound healing molecules, and the local inflammatory milieu that regulates their function within the injured CNS remains poorly understood.

Given the recently appreciated and tremendous plasticity of myeloid cells (i.e. classically activated pro-inflammatory M1 monocytes, alternatively activated M2 monocytes, myeloid-derived suppressor cells) (Sica and Mantovani, 2012), the difficulty to specifically target these subpopulations, and treatment paradigms that globally inhibit or augment their response, may underlie the many discrepancies with regards to the role of macrophages in the field of CNS injury (David and Kroner, 2011). Thus, a better understanding of these divergent subpopulations of microglia/macrophages and their function in the injured CNS setting will be necessary to maximize wound healing and regenerative processes without causing overt neurotoxicity. At present there is no absolute way to separate the microglial response from hematogenous macrophages experimentally or after human SCI. Because of this limitation, our knowledge of the role of resident CNS microglia in

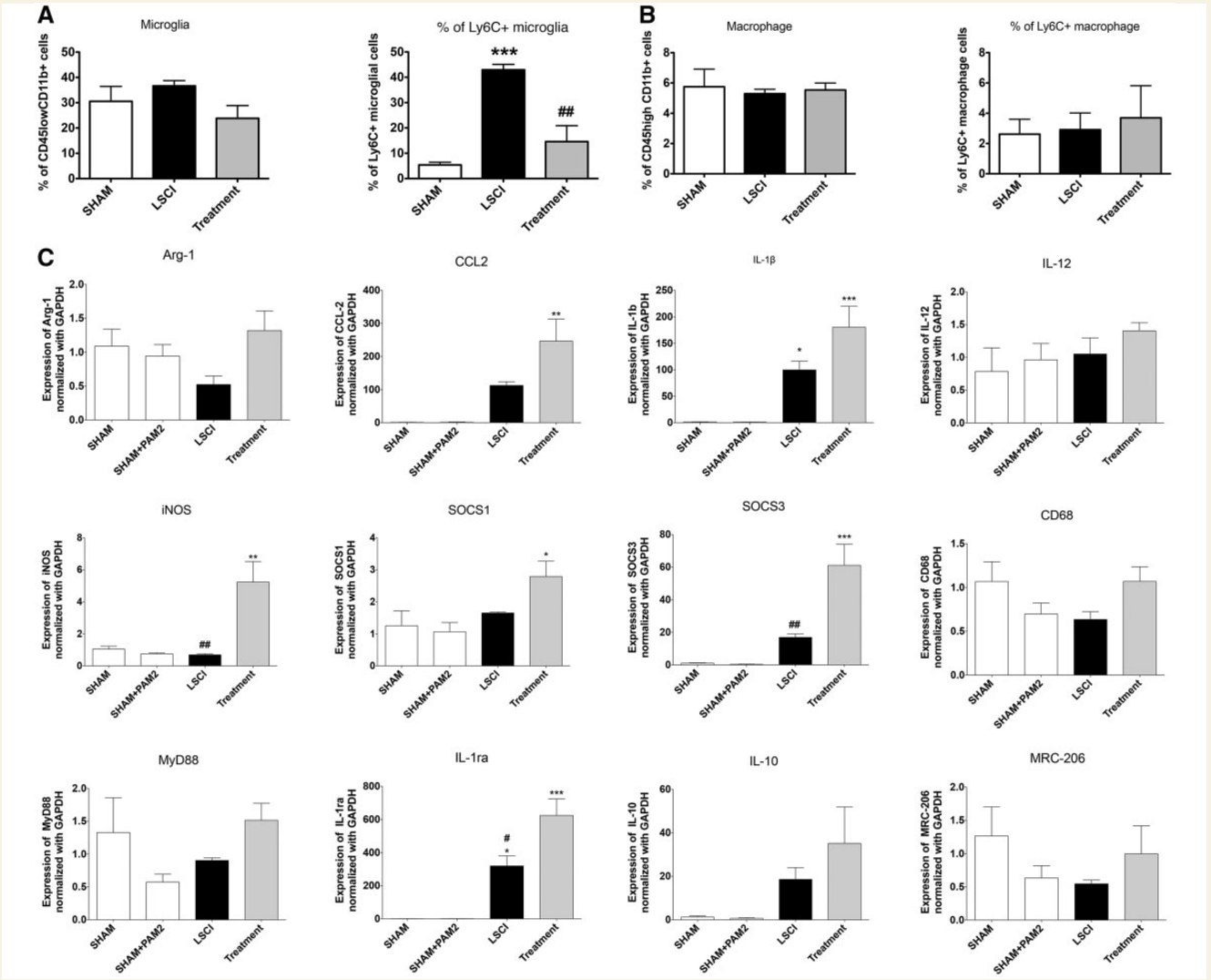

Figure 9 Pam2CSK4 modulation of microglia alters the inflammatory milieu following laser-induced SCI. (**A**) Flow cytometry was used to quantify phenotypic markers of pro-inflammatory microglia and macrophages isolated from the spinal cord 4 h after laser-induced SCI. The % of $CD45^{low}$: CD11b+ microglia did not change versus sham injured controls (*left* panel). In contrast, the % of pro-inflammatory microglia, M1 ($CD45^{low}$: CD11b+: Ly6C+) significantly ($P < 0.001$) increased in the laser-induced SCI control spinal cords versus sham treated animals. However, Pam2CSK4 treatment significantly ($P < 0.01$) reduced the % of inflammatory microglia versus endotoxin control treated cords to near control levels. (**B**) CD45high:CD11b and inflammatory macrophage ($CD45^{high}$:CD11b:Ly6C+) response after laser-induced SCI is unchanged between the treated groups and controls. (**C**) Quantitative reverse transcription-PCR reveals that Pam2CSK4 treatment alters pro-inflammatory (M1) and anti-inflammatory (M2-like) messenger RNA levels at 4 h after laser-induced SCI. Pam2CSK4 treatment significantly increases proinflammatory markers CCL2, IL-1b and inducible nitric oxide synthase (iNOS) levels while simultaneously increasing anti-inflammatory markers such as SOCS1 and -3 and IL-1ra versus sham injured cords. Pam2CSK4 treatment significantly increased levels of inducible nitric oxide synthase, SOCS3 and IL-1ra. Data are expressed as mean ± SEM. Pam2CSK4 treatment of sham control spinal cord did not affect gene expression. Statistical significance was assessed using a one-way ANOVA with Tukey's method for multiple comparisons, $*P < 0.01$; $**P < 0.001$; $***P < 0.0001$ (sham compared to all) #laser-induced SCI versus Pam2CSK4, $n = 4$ animals/group.

SCI in general is poorly understood. Thus we purposely developed this *ex vivo* model to better understand the role of microglia in white matter injury, without the confounding effects of blood-derived myeloid responses. By understanding the unique roles of CNS-resident versus blood-borne cells in more detail may encourage or discourage manipulations to target individual subsets depending on the magnitude and effect of each macrophage compartment.

Using two-photon excitation time-lapse video microscopy and spectral microscopy, we demonstrated that microglia rapidly respond to laser-induced SCI by extending their processes to presumably seal off the lesion area as previously shown following penetrating brain injury (Hines *et al*., 2009). These results are in agreement with a previous study that assessed the microglial response to SCI *in vivo* suggestive that the *ex vivo* model used here recapitulates the microglial response *in vivo* (Dibaj *et al*., 2010).

Our model of axonal injury also closely mimics the axonopathy described in well-characterized clinically relevant models of SCI including contusive, compressive, and transection based models. In support, dorsal column transection *in vivo* induces endbulb formation on transected ascending sensory fibres with morphologies identical to ours (Erturk *et al*., 2007). These structures often appear round and/or oval at the proximal cut end of the axon with diameters larger than the proximal axonal shaft with no growth-cone like extensions [*c.f.* Fig. 1F and G in Erturk *et al*. (2007) using an *in vivo* transection SCI model with our data in Figs 1C, D and 5A].

Similarly, acute ultrastructural studies reported that at 4 h after weight drop contusion SCI, the formation of 'terminal clubs' or endbulbs represented severed axons and were scattered predominantly in white matter (Wagner *et al*., 1978). Alike to contusion SCI, proximal stubs of sheared or transected axons formed swollen endbulbs (retraction bulbs) identical to what we describe in our laser-induced SCI model (Kao *et al*., 1977). Moreover, in a quantitative assessment of acute changes in axonal injury following spinal cord compression injury, Anthes *et al*. (1995) described several axonal changes especially within the first few hours after injury. These were peri-axonal swelling (i.e. an increase in the periaxonal space between the axolemma and surrounding myelin sheath), myelin vesiculation and rupturing, organelle accumulation in axons surrounding a neurofilamentous axonal core, and terminal swollen axonal endbulbs. Of note, terminal endbulb formation, swollen myelin, and periaxonal swelling, are key features of acute pathological changes in axons following our laser-induced SCI model (see Fig. 5 for example). Lastly, axonal spheroid formation and axonal endbulb formation has been recognized previously in both compressive, contusive, and transection based SCI models (Kao *et al*., 1977; Balentine, 1978; Bresnahan, 1978) and is thought to result from the injury itself, or subsequent resealing of sheared, ruptured or transected axons and accumulation of organelles (Anthes *et al*., 1995). Thus, our laser-induced SCI model mimics acute axonal changes seen in more clinically relevant models of SCI; however, the spatiotemporal precision and submicron level of resolution in our model is a major advantage and allows direct visualization of these dynamic changes as they are occurring in real-time, not possible with assessments of static sections.

Here we reveal that the microglial response to laser-induced SCI occurred in parallel to secondary axonal degeneration in real time and microglial processes were intimately associated with axonal dieback and secondary axonal degeneration, and ballooning myelin. We also found that spectral microscopy is a powerful tool to visualize spectral shifts in solvatochromatic fluorescent dyes such as Nile Red, whose fluorescence is highly dependent on the polarity of its environment and can be used to differentially detect highly lipophilic structures such as myelin, and the unveiling of hydrophobic protein surfaces (Sackett and Wolff, 1987) that likely appear in endbulbs after injury.

In support, we uncover a novel spectral shift in the emission of Nile Red between axonal endbulbs, undergoing axonal dieback and myelin that can be spectrally resolved to allow specific visualization and changes in these structures as they undergo degeneration. These Nile Red spectral changes in endbulbs may represent accumulation of proteins (e.g. amyloid precursor protein) or the hydrophobic surfaces of tubulin that are known to be present in stumps of transected axons acutely during endbulb formation (Sackett *et al*., 1990; Erturk *et al*., 2007). Equally important is the ability to differentiate between several closely overlapping emission spectra (i.e. YFP, GFP) allowing the unequivocal identification of several cell types simultaneously within the injured CNS. Further work using these novel tools will be necessary to determine the identity and significance of these acute pathological changes in axons following injury in real-time.

Counter to our hypothesis, microglia modulation through sterile targeting of TLR2 receptors using Pam2CSK4 greatly increased the microglial response to laser-induced SCI, altered the inflammatory milieu of the injured spinal cord, but surprisingly reduced secondary degeneration of myelinated fibres. These neuroprotective outcomes after Pam2CSK4 treatment were associated with reduced Ly6C expression (a common marker of M1 pro-inflammatory monocytes) in microglia and a mixed phenotype of M1:M2 (both pro and anti-inflammatory) molecules isolated from injured white matter. However, it is important to note that our analyses were largely at 4 h after injury, an early time point where markers of protein expression such as MHCII, CD80 and CD86 are all likely to be inconclusive to completely resolve M1 and M2 phenotype. Thus, we resorted to PCR analyses, as messenger RNA changes precede protein alterations for the markers presented in Fig. 9. Our data indicate that M1 and M2 markers are both elevated at the 4-h time point, indicating that at this very early period of injury *ex vivo*, M1 and M2 transcripts are concordantly elevated; it is possible that mixed elevation occurs at early periods (hours) after injury, and that it is not reported by others as their analyses typically involve specimens collected days after the insult (Kigerl *et al*., 2009).

Interestingly, Pam2CSK4 treatment induced upregulation of inducible nitric oxide synthase and presumably induced release of nitric oxide and other pro-inflammatory molecules (e.g. IL1B) (Fig. 9) that have been previously shown to contribute to CNS injury (David and Kroner, 2011). Although the newly described Ly6C^{low}: inducible nitric oxide synthase-positive macrophages may contribute to secondary degeneration at later time-points after SCI (Donnelly *et al*., 2011), the Pam2CSK4-induced inducible nitric oxide synthase expressing microglia acutely after SCI (current study) may be beneficial by sealing of the lesion site and preventing secondary degeneration. In support, nitric oxide regulates white matter spinal cord microglial process extension towards sites of injury *in vivo* (Dibaj *et al*., 2010) and inhibiting microglial process extension exacerbates lesion size after brain injury (Hines *et al*., 2009).

Concurrently to M1 marker expression, potent anti-inflammatory molecules (i.e. SOCS1 and 3 and IL-1ra) were significantly increased in Pam2CSK4 treated animals versus controls. The suppressor of cytokine signalling (SOCS) proteins are potent attenuators of TLR mediated responses in immune cells (Baker *et al*., 2009), and IL-1ra is a potent inhibitor of IL1B signalling and prevents IL1B induced white matter injury after SCI (Nesic *et al*., 2001). Thus Pam2CSK4-induced upregulation of SOCS and IL-1ra may downregulate the release of microglial-derived toxins and M1-like macrophage polarization. Collectively, the

increase in both M1 and M2 markers and lack of blood-derived monocytes suggest a novel functional alternatively activated microglial phenotype that can be modulated *in situ* and is associated with reduced secondary white matter injury. Importantly, we found no evidence to support a pure M1 or M2 phenotype in microglia at 4 h after laser-induced SCI but rather a mixed phenotype within the two extremes as both M1-like and M2-like markers were present and there was no distinction between Ly6C^{high} and Ly6C^{low} expression in living spinal cord as has been shown for monocytes in peripheral tissues. Although microglia were the focus of this study and respond robustly to TLR agonists in brain (Rivest, 2003), it is important to note that we cannot exclude the possible contribution of other glial cells to acute axonal injury. However, controversy exists with regards to astrocyte expression of TLR2, pro-inflammatory and chemokine transcripts are typically localized to microglia within the first few hours of immune challenge or CNS injury (Babcock *et al*., 2003; Rivest, 2003), and endothelial cells weakly respond to TLR2 agonists (Faure *et al*., 2000). Future studies will be needed to examine the interactions between microglia and astrocytes as the former can influence the latter's response to inflammatory stimuli.

In contrast to these results, treatments that have been previously shown to inhibit microglial mediated release of neurotoxic molecules (i.e. carbenoxolone and L-AP4) failed to protect the injured spinal cord in the current study and are at odds with previous *in vitro* and *in vivo* studies that have shown that microglia contribute to white matter injury (Park *et al*., 2004; Takeuchi *et al*., 2005; Domercq *et al*., 2007, Pinteaux-Jones *et al*., 2008). Although the reasons behind these discrepancies remain unknown, it is possible that in our *ex vivo* model the microglial release of potentially neurotoxic molecules is tightly regulated by factors released by surrounding cells (Aguzzi *et al*., 2013); therefore, neurotoxin release may be dampened compared with TLR agonist stimulation of microglia *in vitro* that lacks this regulation. Therefore, under these conditions it is plausible that L-AP4 and carbenoxolone would have no obvious effect. Alternatively, given the acute endpoint in our study, we may have missed subsequent release of potential neurotoxic molecules at later time-points that may have induced white matter injury. These discrepancies may also underlie the important pathological role that blood-derived macrophages may play *in vivo* at later time points following CNS injury and the need for *ex vivo* and *in vivo* models to interrogate the true role of microglia in white matter injury as the local environment likely shapes their response which is unobtainable in cell culture based paradigms.

Although our laser-induced SCI model mimics axonopathy of well-characterized *in vivo* SCI models (as discussed above), we cannot exclude a potential priming effect on microglia and axons as the spinal cord was extracted and thus the response to a subsequent injury (i.e. laser-induced SCI) may be altered. Nonetheless, several observations counter this conclusion. First, a key indicator of CNS trauma or disease is microglia themselves that undergo stereotypical changes in their morphology as they respond to CNS disturbances (Ransohoff and Perry, 2009). As shown in our live imaging studies (Fig. 2), microglia had highly ramified processes that extended and retracted over time and appeared identical to those shown following *in vivo* observations of the exposed brain or spinal cord (Davalos *et al*., 2005; Nimmerjahn *et al*., 2005; Hines *et al*., 2009; Dibaj *et al*., 2010), and in tissue sections from non-injured spinal cord (Stirling and Yong, 2008). Second, following laser-induced injury in brain and spinal cord *in vivo* or following pin-prick injury, microglia become activated and send out their processes to seal of the injury site (Davalos *et al*., 2005; Nimmerjahn *et al*., 2005; Hines *et al*., 2009; Dibaj *et al*., 2010). The spatiotemporal microglial responses in these models are identical in magnitude to the current study. Third, in non-injured conditions in the present study key inflammatory markers were at low or undetectable levels as were markers of microglial activation (Fig. 9 in the current study) parallel to controls used for *in vivo* contusive SCI studies (McTigue *et al*., 1998; Lee *et al*., 2000; Pineau and Lacroix, 2007; Rice *et al*., 2007). Thus, microglia seem not to be activated, nor are inflammatory markers present in this model initially, but both increase after laser-induced SCI as they do following other well-characterized SCI models (Lee *et al*., 2000; Diaz-Ruiz *et al*., 2002; Yang *et al*., 2005; Pineau and Lacroix, 2007). Lastly, axon injury responses such as swelling, spheroid formation, and axonal endbulb formation occurred at similar time-points (within 2–3 h) as shown after *in vivo* compressive or contusive SCI injuries (Kao *et al*., 1977; Balentine, 1978; Anthes *et al*., 1995). Collectively, the lack of microglia activation, inflammatory markers, and similar time course of inflammatory reactions and axonal changes in our laser-induced SCI as shown for contusion SCI *in vivo* suggest the removal of the spinal cord and loss of descending responses from the brain did not significantly impact the results of our study at least at the time-points examined.

In summary, we imaged microglial activation and subsequent axon and myelin pathology in real-time using advanced imaging techniques such as two-photon microscopy and spectral microscopy. We developed a powerful injury model, laser-induced SCI, that allows one to document dynamic processes such as axonal dieback and secondary degeneration of spared fibres with excellent spatio-temporal resolution. Together, these data strongly suggest that promoting beneficial sterile inflammation by the TLR2 agonist Pam2CSK4, induces a robust microglial response that is neuroprotective after laser-induced SCI. Thus, inhibiting the microglial response acutely after SCI with anti-inflammatory treatments may be counter-intuitive, as revealed for L-AP4 and carbenoxolone in the current study.

Importantly, the laser-induced SCI model combined with fluorescent proteins and lipophilic fluorescent dyes allows one to clearly distinguish primary from secondary degeneration, which is difficult to accomplish using other *in vivo* models. It therefore may provide an important stepping-stone to quickly and accurately test the effects of putative neuroprotective agents and document the dynamic changes in axons and myelin as these events are unfolding in real time. Ultimately, the results from the current work have identified TLR2 stimulation of microglia as a novel therapeutic target for SCI. In addition, we provide the rationale to further test the efficacy of Pam2CSK4, and other TLR2 agonists, in delayed treatment paradigms using more clinically relevant models of SCI in which behavioural outcomes can be assessed and thereby rule out potential limitations in the current model such as the lack of blood-derived factors and immune cell

recruitment that may alter the response of microglia to TLR2 stimulation. There is a great need for efficacious neuroprotective treatments for patients with SCI. TLR2 agonists have also entered clinical trials (e.g. NCT01685489) for treating cancer and other conditions, and results from trials of TLR2 agonists have revealed both safety and efficacy in humans (Schmidt *et al*., 2007; Niebuhr *et al*., 2008). It is hoped that the results of this study may lead to the development of more effective neuroprotective treatments for patients with SCI.

Funding

P.K.S: The Leblanc Chair In Spinal Cord Research, CRC, AHFMR. D.P.S. was supported by a grant from the Paralyzed Veterans of America Research Foundation. V.W.Y. acknowledges operating grant funding from the Canadian Institutes of Health Research and NeuroScience Canada, and salary support from the Canada Research Chair program. M.M. acknowledges fellowship support from Alberta Innovates – Health Solutions.

Supplementary material

Supplementary material is available at *Brain* online.

References

Aguzzi A, Barres BA, Bennett ML. Microglia: scapegoat, saboteur, or something else? Science 2013; 339: 156–61.

Ahmed Z, Aslam M, Lorber B, Suggate EL, Berry M, Logan A. Optic nerve and vitreal inflammation are both RGC neuroprotective but only the latter is RGC axogenic. Neurobiol Dis 2010; 37: 441–54.

Anthes DL, Theriault E, Tator CH. Characterization of axonal ultrastructural pathology following experimental spinal cord compression injury. Brain Res 1995; 702: 1–16.

Babcock AA, Kuziel WA, Rivest S, Owens T. Chemokine expression by glial cells directs leukocytes to sites of axonal injury in the CNS. J Neurosci 2003; 23: 7922–30.

Baker BJ, Akhtar LN, Benveniste EN. SOCS1 and SOCS3 in the control of CNS immunity. Trends Immunol 2009; 30: 392–400.

Balentine JD. Pathology of experimental spinal cord trauma. II. Ultrastructure of axons and myelin. Lab Invest 1978; 39: 254–66.

Bao F, Chen Y, Dekaban GA, Weaver LC. Early anti-inflammatory treatment reduces lipid peroxidation and protein nitration after spinal cord injury in rats. J Neurochem 2004; 88: 1335–44.

Blight AR. Effects of silica on the outcome from experimental spinal cord injury: implication of macrophages in secondary tissue damage. Neuroscience 1994; 60: 263–73.

Bresnahan JC. An electron-microscopic analysis of axonal alterations following blunt contusion of the spinal cord of the rhesus monkey (Macaca mulatta). J Neurol Sci 1978; 37: 59–82.

Brown GD, Herre J, Williams DL, Willment JA, Marshall AS, Gordon S. Dectin-1 mediates the biological effects of beta-glucans. J Exp Med 2003; 197: 1119–24.

Byrnes KR, Stoica B, Riccio A, Pajoohesh-Ganji A, Loane DJ, Faden AI. Activation of metabotropic glutamate receptor 5 improves recovery after spinal cord injury in rodents. Ann Neurol 2009; 66: 63–74.

Davalos D, Grutzendler J, Yang G, Kim JV, Zuo Y, Jung S, et al. ATP mediates rapid microglial response to local brain injury *in vivo*. Nat Neurosci 2005; 8: 752–8.

David S, Kroner A. Repertoire of microglial and macrophage responses after spinal cord injury. Nature Rev Neurosci 2011; 12: 388–99.

Diaz-Ruiz A, Ibarra A, Perez-Severiano F, Guizar-Sahagun G, Grijalva I, Rios C. Constitutive and inducible nitric oxide synthase activities after spinal cord contusion in rats. Neurosci lett 2002; 319: 129–32.

Dibaj P, Nadrigny F, Steffens H, Scheller A, Hirrlinger J, Schomburg ED, et al. NO mediates microglial response to acute spinal cord injury under ATP control *in vivo*. Glia 2010; 58: 1133–44.

Domercq M, Sanchez-Gomez MV, Sherwin C, Etxebarria E, Fern R, Matute C. System xc- and glutamate transporter inhibition mediates microglial toxicity to oligodendrocytes. J Immunol 2007; 178: 6549–56.

Donnelly DJ, Longbrake EE, Shawler TM, Kigerl KA, Lai W, Tovar CA, et al. Deficient CX3CR1 signaling promotes recovery after mouse spinal cord injury by limiting the recruitment and activation of Ly6Clo/iNOS+ macrophages. J Neurosci 2011; 31: 9910–22.

Dusart I, Schwab ME. Secondary cell death and the inflammatory reaction after dorsal hemisection of the rat spinal cord. Euro J Neurosci 1994; 6: 712–24.

Erturk A, Hellal F, Enes J, Bradke F. Disorganized microtubules underlie the formation of retraction bulbs and the failure of axonal regeneration. J Neurosci 2007; 27: 9169–80.

Faure E, Equils O, Sieling PA, Thomas L, Zhang FX, Kirschning CJ, et al. Bacterial lipopolysaccharide activates NF-kappaB through toll-like receptor 4 (TLR-4) in cultured human dermal endothelial cells. Differential expression of TLR-4 and TLR-2 in endothelial cells. J Bio Chem 2000; 275: 11058–63.

Feng G, Mellor RH, Bernstein M, Keller-Peck C, Nguyen QT, Wallace M, et al. Imaging neuronal subsets in transgenic mice expressing multiple spectral variants of GFP. Neuron 2000; 28: 41–51.

Fitch MT, Doller C, Combs CK, Landreth GE, Silver J. Cellular and molecular mechanisms of glial scarring and progressive cavitation: *in vivo* and *in vitro* analysis of inflammation-induced secondary injury after CNS trauma. J Neurosci 1999; 19: 8182–98.

Giulian D, Vaca K, Corpuz M. Brain glia release factors with opposing actions upon neuronal survival. J Neurosci 1993; 13: 29–37.

Gordon S. Alternative activation of macrophages. Nat Rev Immunol 2003; 3: 23–35.

Guerrero AR, Uchida K, Nakajima H, Watanabe S, Nakamura M, Johnson WE, et al. Blockade of interleukin-6 signaling inhibits the classic pathway and promotes an alternative pathway of macrophage activation after spinal cord injury in mice. J Neuroinflammation 2012; 9: 40.

Hauk TG, Leibinger M, Muller A, Andreadaki A, Knippschild U, Fischer D. Stimulation of axon regeneration in the mature optic nerve by intravitreal application of the toll-like receptor 2 agonist Pam3Cys. Invest Ophthalmol Vis Sci 2010; 51: 459–64.

Hines DJ, Hines RM, Mulligan SJ, Macvicar BA. Microglia processes block the spread of damage in the brain and require functional chloride channels. Glia 2009; 57: 1610–8.

Horn KP, Busch SA, Hawthorne AL, van Rooijen N, Silver J. Another barrier to regeneration in the CNS: activated macrophages induce extensive retraction of dystrophic axons through direct physical interactions. J Neurosci 2008; 28: 9330–41.

Jung S, Aliberti J, Graemmel P, Sunshine MJ, Kreutzberg GW, Sher A, et al. Analysis of fractalkine receptor CX(3)CR1 function by targeted deletion and green fluorescent protein reporter gene insertion. Mol Cell Biol 2000; 20: 4106–14.

Kao CC, Chang LW, Bloodworth JM Jr. Electron microscopic observations of the mechanisms of terminal club formation in transected spinal cord axons. J Neuropathol Exp Neurol 1977; 36: 140–56.

Kawai T, Akira S. The role of pattern-recognition receptors in innate immunity: update on Toll-like receptors. Nat Immunol 2010; 11: 373–84.

Kigerl KA, Lai W, Rivest S, Hart RP, Satoskar AR, Popovich PG. Toll-like receptor (TLR)-2 and TLR-4 regulate inflammation, gliosis, and myelin sparing after spinal cord injury. J Neurochem 2007; 102: 37–50.

Kigerl KA, Gensel JC, Ankeny DP, Alexander JK, Donnelly DJ, Popovich PG. Identification of two distinct macrophage subsets with

divergent effects causing either neurotoxicity or regeneration in the injured mouse spinal cord. J Neurosci 2009; 29: 13435–44.
Lee YL, Shih K, Bao P, Ghirnikar RS, Eng LF. Cytokine chemokine expression in contused rat spinal cord. Neurochem Int 2000; 36: 417–25.
Lehnardt S, Lachance C, Patrizi S, Lefebvre S, Follett PL, Jensen FE, et al. The toll-like receptor TLR4 is necessary for lipopolysaccharide-induced oligodendrocyte injury in the CNS. J Neurosci 2002; 22: 2478–86.
Lehnardt S. Innate immunity and neuroinflammation in the CNS: the role of microglia in Toll-like receptor-mediated neuronal injury. Glia 2010; 58: 253–63.
Leon S, Yin Y, Nguyen J, Irwin N, Benowitz LI. Lens injury stimulates axon regeneration in the mature rat optic nerve. J Neurosci 2000; 20: 4615–26.
Long EM, Millen B, Kubes P, Robbins SM. Lipoteichoic acid induces unique inflammatory responses when compared to other toll-like receptor 2 ligands. PloS One 2009; 4: e5601.
McTigue DM, Tani M, Krivacic K, Chernosky A, Kelner GS, Maciejewski D, et al. Selective chemokine mRNA accumulation in the rat spinal cord after contusion injury. J Neurosci Res 1998; 53: 368–76.
Mishra MK, Wang J, Silva C, Mack M, Yong VW. Kinetics of proinflammatory monocytes in a model of multiple sclerosis and its perturbation by laquinimod. Am J Pathol 2012; 181: 642–51.
Nesic O, Xu GY, McAdoo D, High KW, Hulsebosch C, Perez-Pol R. IL-1 receptor antagonist prevents apoptosis and caspase-3 activation after spinal cord injury. J Neurotrauma 2001; 18: 947–56.
Niebuhr M, Muhlradt PF, Wittmann M, Kapp A, Werfel T. Intracutaneous injection of the macrophage-activating lipopeptide-2 (MALP-2) which accelerates wound healing in mice–a phase I trial in 12 patients. Exp Dermatol 2008; 17: 1052–6.
Nimmerjahn A, Kirchhoff F, Helmchen F. Resting microglial cells are highly dynamic surveillants of brain parenchyma *in vivo*. Science 2005; 308: 1314–8.
Oudega M, Vargas CG, Weber AB, Kleitman N, Bunge MB. Long-term effects of methylprednisolone following transection of adult rat spinal cord. Euro J Neurosci 1999; 11: 2453–64.
Park E, Velumian AA, Fehlings MG. The role of excitotoxicity in secondary mechanisms of spinal cord injury: a review with an emphasis on the implications for white matter degeneration. J Neurotrauma 2004; 21: 754–74.
Pineau I, Lacroix S. Proinflammatory cytokine synthesis in the injured mouse spinal cord: multiphasic expression pattern and identification of the cell types involved. J Comp Neurol 2007; 500: 267–85.
Pinteaux-Jones F, Sevastou IG, Fry VA, Heales S, Baker D, Pocock JM. Myelin-induced microglial neurotoxicity can be controlled by microglial metabotropic glutamate receptors. J Neurochem 2008; 106: 442–54.
Popovich PG, Guan Z, McGaughy V, Fisher L, Hickey WF, Basso DM. The neuropathological and behavioral consequences of intraspinal microglial/macrophage activation. J Neuropath Exp Neurol 2002; 61: 623–33.
Popovich PG, Guan Z, Wei P, Huitinga I, van Rooijen N, Stokes BT. Depletion of hematogenous macrophages promotes partial hindlimb recovery and neuroanatomical repair after experimental spinal cord injury. Exp Neurol 1999; 158: 351–65.
Prewitt CM, Niesman IR, Kane CJ, Houle JD. Activated macrophage/microglial cells can promote the regeneration of sensory axons into the injured spinal cord. Exp Neurol 1997; 148: 433–43.
Rabchevsky AG, Streit WJ. Grafting of cultured microglial cells into the lesioned spinal cord of adult rats enhances neurite outgrowth. J Neurosci Res 1997; 47: 34–48.
Ransohoff RM, Perry VH. Microglial physiology: unique stimuli, specialized responses. Ann Rev Immunol 2009; 27: 119–45.
Rapalino O, Lazarov-Spiegler O, Agranov E, Velan GJ, Yoles E, Fraidakis M, et al. Implantation of stimulated homologous macrophages results in partial recovery of paraplegic rats. Nat Med 1998; 4: 814–21.
Rice T, Larsen J, Rivest S, Yong VW. Characterization of the early neuroinflammation after spinal cord injury in mice. J Neuropathol Exp Neurol 2007; 66: 184–95.
Rivest S. Molecular insights on the cerebral innate immune system. Brain Behav Immun 2003; 17: 13–9.
Sackett DL, Wolff J. Nile red as a polarity-sensitive fluorescent probe of hydrophobic protein surfaces. Anal Biochem 1987; 167: 228–34.
Sackett DL, Knutson JR, Wolff J. Hydrophobic surfaces of tubulin probed by time-resolved and steady-state fluorescence of nile red. J Biol Chem 1990; 265: 14899–906.
Satake K, Matsuyama Y, Kamiya M, Kawakami H, Iwata H, Adachi K, et al. Nitric oxide via macrophage iNOS induces apoptosis following traumatic spinal cord injury. Brain Res Mol Brain Res 2000; 85: 114–22.
Schmidt J, Welsch T, Jager D, Muhlradt PF, Buchler MW, Marten A. Intratumoural injection of the toll-like receptor-2/6 agonist 'macrophage-activating lipopeptide-2' in patients with pancreatic carcinoma: a phase I/II trial. Br J Cancer 2007; 97: 598–604.
Sica A, Mantovani A. Macrophage plasticity and polarization: *in vivo* veritas. J Clin Invest 2012; 122: 787–95.
Stirling DP, Khodarahmi K, Liu J, McPhail LT, McBride CB, Steeves JD, et al. Minocycline treatment reduces delayed oligodendrocyte death, attenuates axonal dieback, and improves functional outcome after spinal cord injury. J Neurosci 2004; 24: 2182–90.
Stirling DP, Yong VW. Dynamics of the inflammatory response after murine spinal cord injury revealed by flow cytometry. J Neurosci Res 2008; 86: 1944–58.
Takeuchi H, Mizuno T, Zhang G, Wang J, Kawanokuchi J, Kuno R, et al. Neuritic beading induced by activated microglia is an early feature of neuronal dysfunction toward neuronal death by inhibition of mitochondrial respiration and axonal transport. J Biol Chem 2005; 280: 10444–54.
Taylor DL, Diemel LT, Pocock JM. Activation of microglial group III metabotropic glutamate receptors protects neurons against microglial neurotoxicity. J Neurosci 2003; 23: 2150–60.
van Bergenhenegouwen J, Plantinga TS, Joosten LA, Netea MG, Folkerts G, Kraneveld AD, et al. TLR2 & Co: a critical analysis of the complex interactions between TLR2 and coreceptors. J leukoc Biol 2013; 94: 885–902.
Wagner FC Jr., VanGilder JC, Dohrmann GJ. Pathological changes from acute to chronic in experimental spinal cord trauma. J Neurosurg 1978; 48: 92–8.
Yang L, Jones NR, Blumbergs PC, Van Den Heuvel C, Moore EJ, Manavis J, et al. Severity-dependent expression of pro-inflammatory cytokines in traumatic spinal cord injury in the rat. J Clin Neurosci 2005; 12: 276–84.
Yawata I, Takeuchi H, Doi Y, Liang J, Mizuno T, Suzumura A. Macrophage-induced neurotoxicity is mediated by glutamate and attenuated by glutaminase inhibitors and gap junction inhibitors. Life Sci 2008; 82: 1111–16.